



Metabolic Strategies Shared by Basement Residents of the Lost City Hydrothermal Field

✉ William J. Brazelton,^a Julia M. McGonigle,^{a,b} Shahrzad Motamed, ^a H. Lizethe Pendleton, ^a Katrina I. Twing,^{a,*} Briggs C. Miller,^a William J. Lowe,^a Alessandrina M. Hoffman,^a Cecilia A. Prator,^a Grayson L. Chadwick,^c Rika E. Anderson,^d Elaina Thomas,^d David A. Butterfield,^e Karmina A. Aquino,^f Gretchen L. Früh-Green,^f Matthew O. Schrenk,^g Susan Q. Lang^h§

^aSchool of Biological Sciences, University of Utah, Salt Lake City, Utah, USA

^bBigelow Laboratory for Ocean Sciences, East Boothbay, Maine, USA

^cDepartment of Molecular and Cell Biology, University of California, Berkeley, California, USA

^dDepartment of Biology, Carleton College, Northfield, Minnesota, USA

^eJoint Institute for the Study of Atmosphere and Ocean, University of Washington, Seattle, Washington, USA

^fDepartment of Earth Sciences, ETH Zurich, Zurich, Switzerland

^gDepartment of Earth and Environmental Sciences, Michigan State University, East Lansing, Michigan, USA

^hSchool of the Earth, Ocean, and Environment, University of South Carolina, Columbia, South Carolina, USA

ABSTRACT Alkaline fluids venting from chimneys of the Lost City hydrothermal field flow from a potentially vast microbial habitat within the seafloor where energy and organic molecules are released by chemical reactions within rocks uplifted from Earth's mantle. In this study, we investigated hydrothermal fluids venting from Lost City chimneys as windows into subseafloor environments where the products of geochemical reactions, such as molecular hydrogen (H_2), formate, and methane, may be the only available sources of energy for biological activity. Our deep sequencing of metagenomes and metatranscriptomes from these hydrothermal fluids revealed a few key species of archaea and bacteria that are likely to play critical roles in the subseafloor microbial ecosystem. We identified a population of *Thermodesulfobacteriales* (belonging to phylum *Nitrospirota*) as a prevalent sulfate-reducing bacterium that may be responsible for much of the consumption of H_2 and sulfate in Lost City fluids. Metagenome-assembled genomes (MAGs) classified as *Methanosaerincaceae* and *Candidatus Bipolaricauota* were also recovered from venting fluids and represent potential methanogenic and acetogenic members of the subseafloor ecosystem. These genomes share novel hydrogenases and formate dehydrogenase-like sequences that may be unique to hydrothermal environments where H_2 and formate are much more abundant than carbon dioxide. The results of this study include multiple examples of metabolic strategies that appear to be advantageous in hydrothermal and subsurface alkaline environments where energy and carbon are provided by geochemical reactions.

IMPORTANCE The Lost City hydrothermal field is an iconic example of a microbial ecosystem fueled by energy and carbon from Earth's mantle. Uplift of mantle rocks into the seafloor can trigger a process known as serpentinization that releases molecular hydrogen (H_2) and creates unusual environmental conditions where simple organic carbon molecules are more stable than dissolved inorganic carbon. This study provides an initial glimpse into the kinds of microbes that live deep within the seafloor where serpentinization takes place, by sampling hydrothermal fluids exiting from the Lost City chimneys. The metabolic strategies that these microbes appear to be using are also shared by microbes that inhabit other sites of serpentinization, including continental subsurface environments and natural springs. Therefore, the results of this study contribute to a broader, interdisciplinary effort to understand the general principles and mechanisms by which serpentinization-associated processes can support life on Earth and perhaps other worlds.

Editor Haruyuki Atomi, Kyoto University

Copyright © 2022 Brazelton et al. This is an open-access article distributed under the terms of the Creative Commons Attribution 4.0 International license.

Address correspondence to William J. Brazelton, william.brazelton@utah.edu.

*Present address: Katrina I. Twing, Department of Microbiology, Weber State University, Ogden, Utah, USA.

§Present address: Susan Q. Lang, Department of Geology and Geophysics, Woods Hole Oceanographic Institution, Woods Hole, Massachusetts, USA.

The authors declare no conflict of interest.

Received 2 June 2022

Accepted 28 July 2022

Published 11 August 2022

KEYWORDS acetogenesis, formate, hydrogenase, hydrothermal, metagenomics, methanogenesis, serpentinization, sulfate reduction

The fixation of carbon dioxide into organic carbon by autotrophic organisms is the foundation of all ecosystems on Earth. Even in subsurface environments, organic carbon is provided by fixation of carbon dioxide by chemoautotrophs or from the degradation of organic carbon originally produced in photosynthetic ecosystems and transported into the subsurface. However, organic carbon can form abiotically in hydrothermal environments, particularly in those that favor a set of geochemical reactions collectively known as serpentinization (1, 2). Microbial communities in serpentinizing environments are likely to benefit from the abiotic synthesis of simple organic compounds, but the processes and mechanisms that may allow this to occur have only recently been studied (3–5).

The Lost City hydrothermal field is located near the summit of the Atlantis Massif, a submarine mountain formed by the uplift of ultramafic rocks from Earth's upper mantle and emplacement onto the seafloor along a major fault zone (6–8). Serpentinization of the Atlantis Massif results in the generation of H₂ and hydrothermal fluids that are rich in formate, methane, and perhaps other forms of organic carbon (9–11). Dissolved inorganic carbon is vanishingly rare in the pH 9 to 11 hydrothermal fluids that vent from Lost City chimneys because it is either reduced to formate or methane, or is precipitated as carbonate minerals (11, 12). Sulfate, in contrast, appears to be an available oxidant throughout the subseafloor because it is never completely consumed by the relatively moderate hydrothermal conditions within the Atlantis Massif (4, 6).

Dense biofilm communities coating the surfaces of Lost City chimneys are capable of utilizing this bounty of energy and carbon released from the mantle (10, 13). However, these biofilms form in mixing zones where warm, anoxic hydrothermal fluids vent into cold, oxic seawater. These conditions may not be representative of subseafloor environments within the Atlantis Massif where habitats are probably confined to sparsely distributed fractures and channels within rocks that have limited exposure to seawater (8, 14). In particular, dissolved inorganic carbon is provided by ambient seawater to chimney biofilm communities, while its availability is severely limited in subseafloor habitats dominated by the products of serpentinization.

The microbiology of fluids venting from Lost City chimneys has been explored in only one study (15), as all other microbiological research at Lost City has focused on the chimney biofilms (4, 9, 10, 13, 16, 17). That early census of microbial diversity identified several novel 16S rRNA gene sequences, but they were poorly classified due to the limitations of microbial taxonomy at the time (15). In particular, the presence of potential sulfate-reducing bacteria (SRB) in Lost City fluids has been a mystery despite clear biogeochemical trends that indicate widespread SRB activity in the subseafloor (4, 10).

A deep-sea expedition to the Lost City in 2018 was designed to fill this knowledge gap by investigating the microbiology and biogeochemistry of fluids venting from Lost City chimneys (18). We exploited natural biogeochemical trends in fluids venting from distinct chimney locations within the Lost City field to test hypotheses about subseafloor microbial metabolic activity. Here, we report initial results from the sequencing of DNA and RNA in Lost City fluids, including the first sequences of metagenomes and metatranscriptomes from Lost City hydrothermal fluids. We identify a few key archaea and bacteria that appear to be indicative of subseafloor habitats strongly influenced by serpentinization. These results highlight metabolic strategies and adaptations that are common to life fueled by the products of serpentinization, including the potential use of formate and other simple forms of organic carbon as the primary sources of carbon for the ecosystem.

RESULTS

Characteristics of Lost City hydrothermal fluid samples. Hydrothermal fluid samples were collected from actively venting chimneys at the Lost City hydrothermal field (Fig. 1; Fig. S1) using ROV *Jason* during the 2018 Lost City expedition aboard R/V

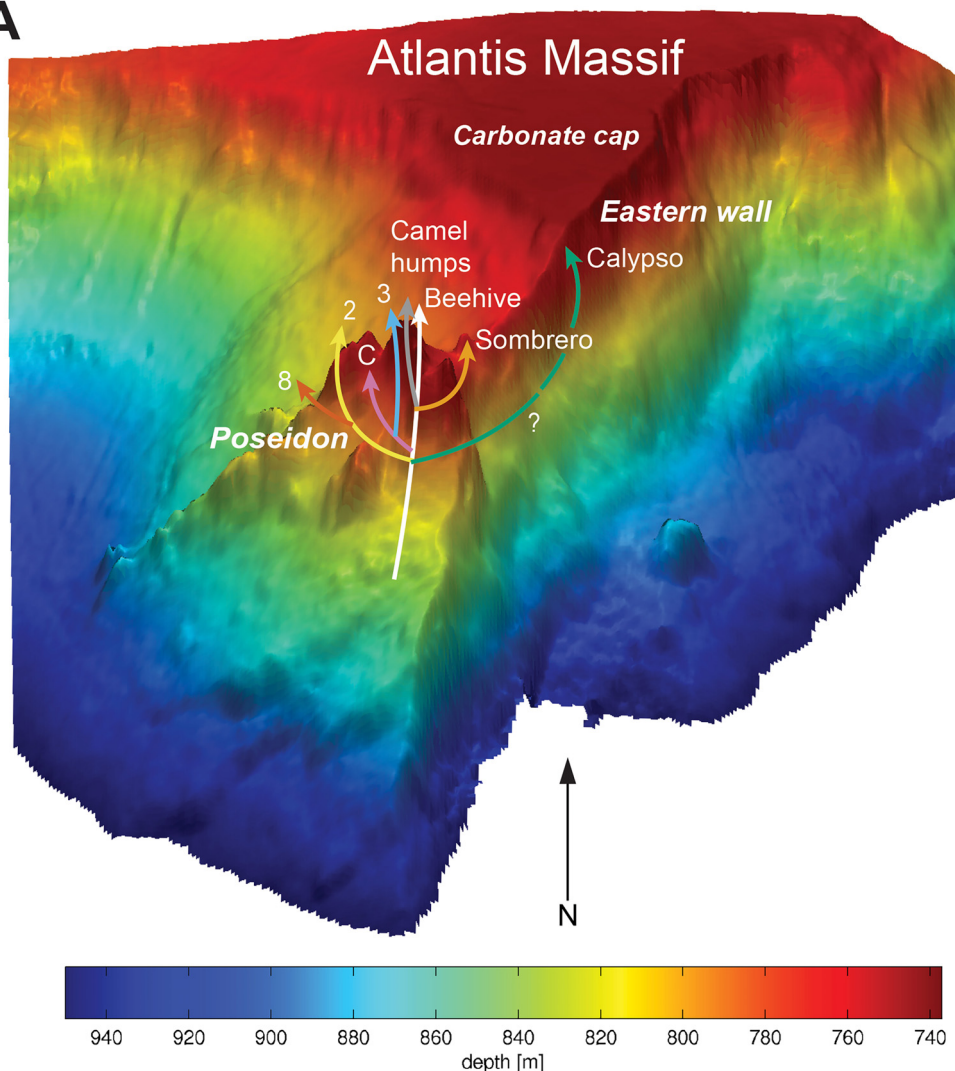
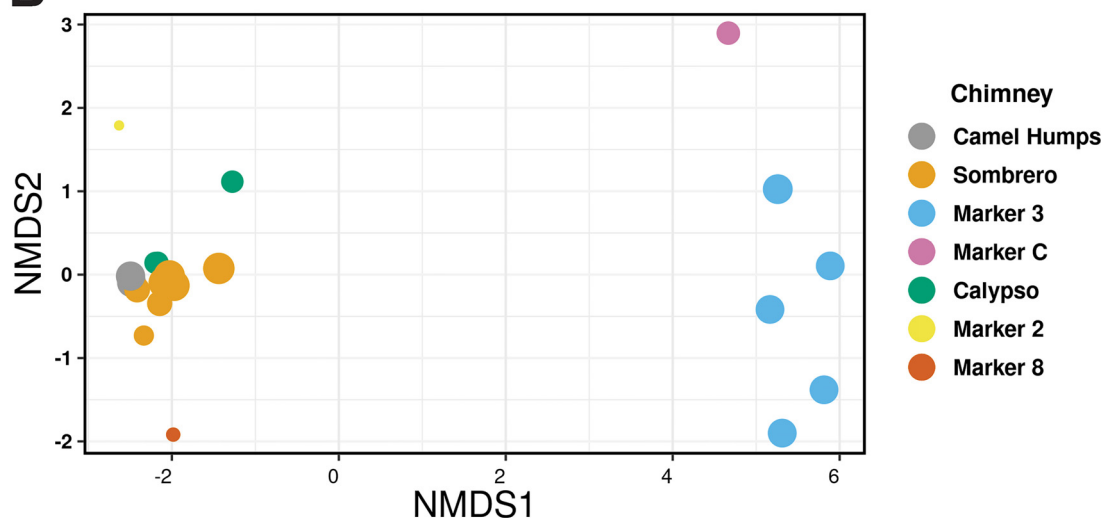
A**B**

FIG 1 The Lost City hydrothermal field is located at 30°N, west of the Mid-Atlantic Ridge, on the southern wall of the Atlantis Massif. Part A shows a three-dimensional view of the field (after Kelley et al., 2005 [6]) featuring the massive Poseidon structure,

(Continued on next page)

TABLE 1 Overview of hydrothermal fluid samples collected from Lost City chimneys

Chimney location	Metagenome libraries	Metatranscriptome libraries	16S rRNA amplicon libraries (DNA)	16S rRNA amplicon libraries (RNA)	Cells per mL ^a	Max T (°C) ^b	pH	Sulfide (mmol/kg)	Sulfate (mmol/kg)	Mg (mmol/kg)
Camel Humps	2	0	4	0	4.3×10^4	41	8.1	0.02	24	47
Sombrero1	3	1	7	1	5.9×10^4	13	8.0	0.002	27	54
Sombrero2	2	0	6	1	6.3×10^4	52	8.7	0.12	18	36
Marker 3	2	0	6	0	6.3×10^4	21	8.6	0.20	23	45
Marker C	0	0	1	1	3.8×10^4	80	10.1	0.39	16	31
Calypso	2	0	6	1	4.8×10^4	24	9.3	1.3	15	30
Marker 2	2	1	3	1	2.6×10^4	58	9.5	1.8	8	15
Marker 8	0	0	1	0	7.5×10^4	42	9.9	1.8	9	19

^aCell numbers are the median of all samples collected from that location.

^bTemperatures and chemistry values are reported for one representative sample collected from that location, typically the sample for which the most chemistry and/or sequence data were available.

Atlantis (AT42-01). This study includes 39 samples of hydrothermal fluids dedicated to DNA and RNA sequencing, including analyses of amplicon sequence variants (ASVs), metagenomes, and metatranscriptomes (Table 1; Table S1).

The fluid samples ranged from those that were barely distinguishable from ambient seawater ($\sim 11^\circ\text{C}$, pH 8) to warm and highly alkaline hydrothermal fluids ($\sim 80^\circ\text{C}$, pH 10). Direct counts of visible cells showed little variability among fluids, with densities approximately 2 to $8 \times 10^4 \text{ mL}^{-1}$ in all samples, although the two samples with the highest temperatures had the least number of cells (Table 1).

Fluids venting from markers 3 and C contained ASV compositions that were notably distinct from those of all other fluids (Fig. 1), including high relative abundances of *Thermodesulfovibronia*, *Desulfotomaculum*, and *Bipolaricaulota* (Fig. 2; Table S2). In addition, marker 3 fluids were rich in metagenomic sequences classified as family *Methanosaerincaceae*, which includes the dominant archaeal phylotype previously detected in Lost City chimneys (16, 17, 19). The greater representation of archaeal sequences in the metagenomes suggests a bias against archaeal sequences in the ASV data set.

Fluids venting from Camel Humps were more diverse than fluids from markers 3 and C ($\sim 4,000$ versus ~ 200 observed ASVs and Inverse Simpson index of approximately 100 to 200 versus 10 to 50; Table S2), and contained likely chimney-associated taxa such as *Sulfurovum*, *Sulfurospirillum*, and *Thiomicrosporadus* (15, 16) at similar abundances as taxa typically associated with ambient seawater (e.g., *Alteromonas*, *Roseobacter*, *Halomonas*). The overall microbial community structure of Sombrero fluids is broadly similar to that of Camel Humps fluids, although warmer and more sulfidic Sombrero fluids included greater proportions of taxa that were also abundant in fluids from markers 3 and C (Fig. 2). Fluid samples from the chimneys at markers 2 and 8 contained a similar combination of chimney-associated and seawater-derived taxa, although marker 2 fluids were particularly dominated by *Alteromonas* and marker 8 fluids by *Sulfurovum* (Table S2).

In general, the proportion of ambient seawater in each hydrothermal fluid sample, as measured by Mg concentration, did not predict the presence of microbes likely to inhabit anoxic, subseafloor environments. Instead, the distribution of anaerobic taxa most likely to be strongly linked with serpentinization (e.g., *Methanosaerincaceae*, *Thermodesulfovibronia*, *Desulfotomaculum*, and *Bipolaricaulota*) was strongly chimney-specific, indicating a strong influence of subsurface conditions that is only weakly mitigated by the mixture of seawater during sampling. Detailed comparisons of the hydrothermal fluid samples are provided in the supplemental material.

Metagenome-assembled genomes. A total of 305 metagenome-assembled genomes (MAGs) with at least 50% estimated completion were recovered from the pooled “all fluids”

FIG 1 Legend (Continued)

which is composed of several actively venting chimneys. Hypothetical flow paths are informed by the aqueous geochemistry results reported here, by Aquino et al. (in review [40]), and by prior studies referenced in the main text. Part B is a nonmetric multidimensional scaling (NMDS) ordination of 16S rRNA amplicon sequence data where each data point represents the microbial community composition of one hydrothermal fluid sample. Sizes of data points are scaled to the measured sulfate concentration of that sample (Table 1).

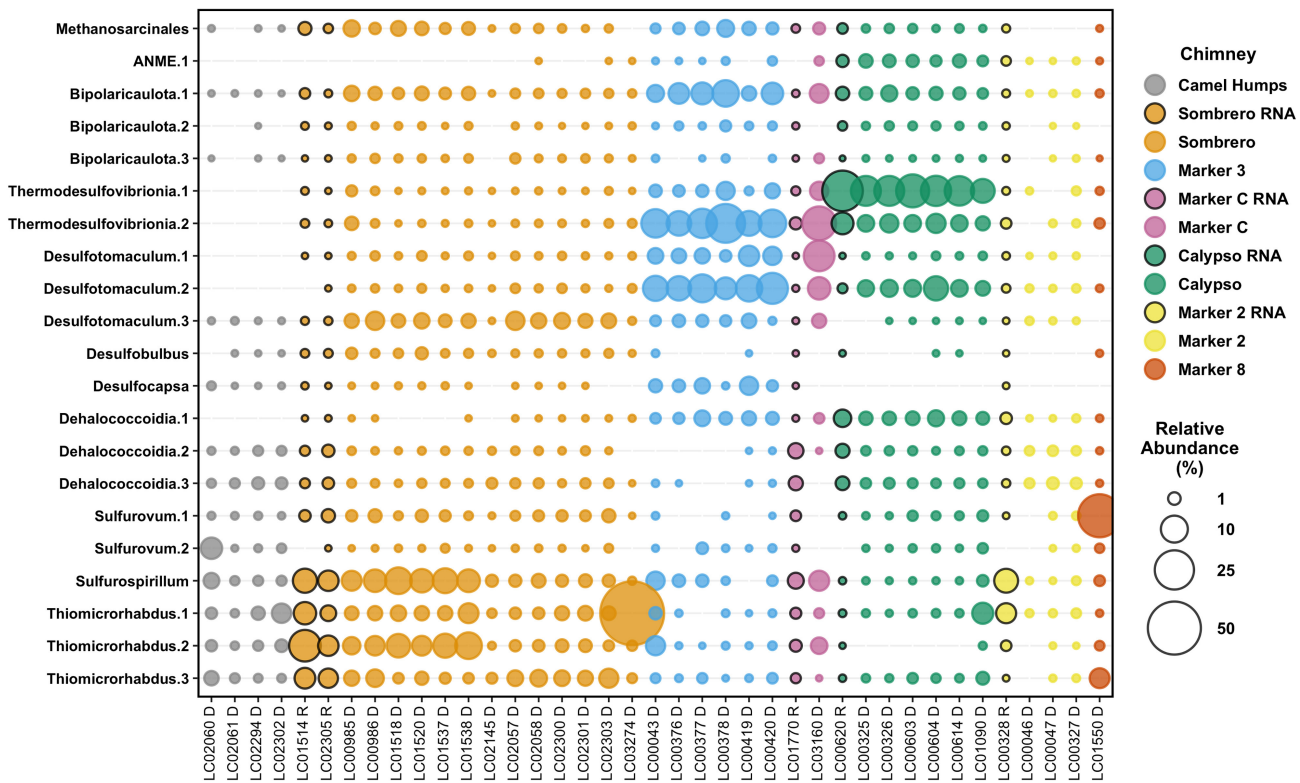


FIG 2 Relative abundances of selected ASVs in Lost City hydrothermal fluid samples. Amplicon libraries were generated from both DNA and RNA extractions; bubbles representing relative abundances in RNA libraries are highlighted with black borders. ASVs were selected to highlight the taxa that were the focus of this study, as well as additional taxa that are expected to be associated with hydrothermal environments and provide context for interpreting differences among fluid samples. A full table of ASV counts is provided in Table S2.

assembly and the six chimney-specific assemblies (Fig. S3; Table S4). MAGs that were representative of the taxa enriched in markers 3 and C, as well as MAGs that contained key genes associated with the metabolism of H₂, sulfate, formate, and methane, were selected for additional analyses. Reassembly and manual refinement of these sequences (see supplemental material) resulted in 30 refined and curated MAGs (Fig. 3) that are at least medium-quality (>50% complete, <10% redundancy, as defined by reference 20). Generally, these MAGs are most abundant in marker 3, Calypso, or Sombrero, and are nearly absent in Camel Humps and marker 2. Unfortunately, metagenomic sequences could not be obtained from marker C or marker 8.

A single *Methanosaerinaeae* MAG that corresponds to the same *Methanosaerinaeae* phylotype previously identified as a dominant member of Lost City chimney biofilm communities (13, 16, 17, 19), was especially abundant in the fluids from marker 3 (Fig. 3; Fig. S5). Although this is the highest-coverage MAG recovered by this study, its maximum coverage of ~6,000 transcripts/fragments per million (TPM) still represents only 0.6% of total mapped reads. Therefore, the few curated MAGs reported here are not an accurate census of the natural microbial community, but they were selected as representatives of the key taxa detected by the 16S rRNA and metagenomic surveys. Many of the 30 refined MAGs share similarities with 16S rRNA and/or metagenomic sequences from other sites associated with serpentinization. In particular, similar *Methanosaerinaeae*, *Thermodesulfovibrionales*, and *Bipolaricaulota* sequences (Fig. S5 to 7) have been identified in chimneys of the Old City and Prony Bay (21, 22).

Below, we briefly describe key features of these MAGs that seem relevant to an initial exploration of the Lost City subseafloor ecosystem, focusing on genes associated with the metabolism of H₂, formate, sulfur, and methane. Additional information about each MAG is reported in the supplemental material, including detailed descriptions of genomic content and predicted protein functions (Tables S5 and 6).

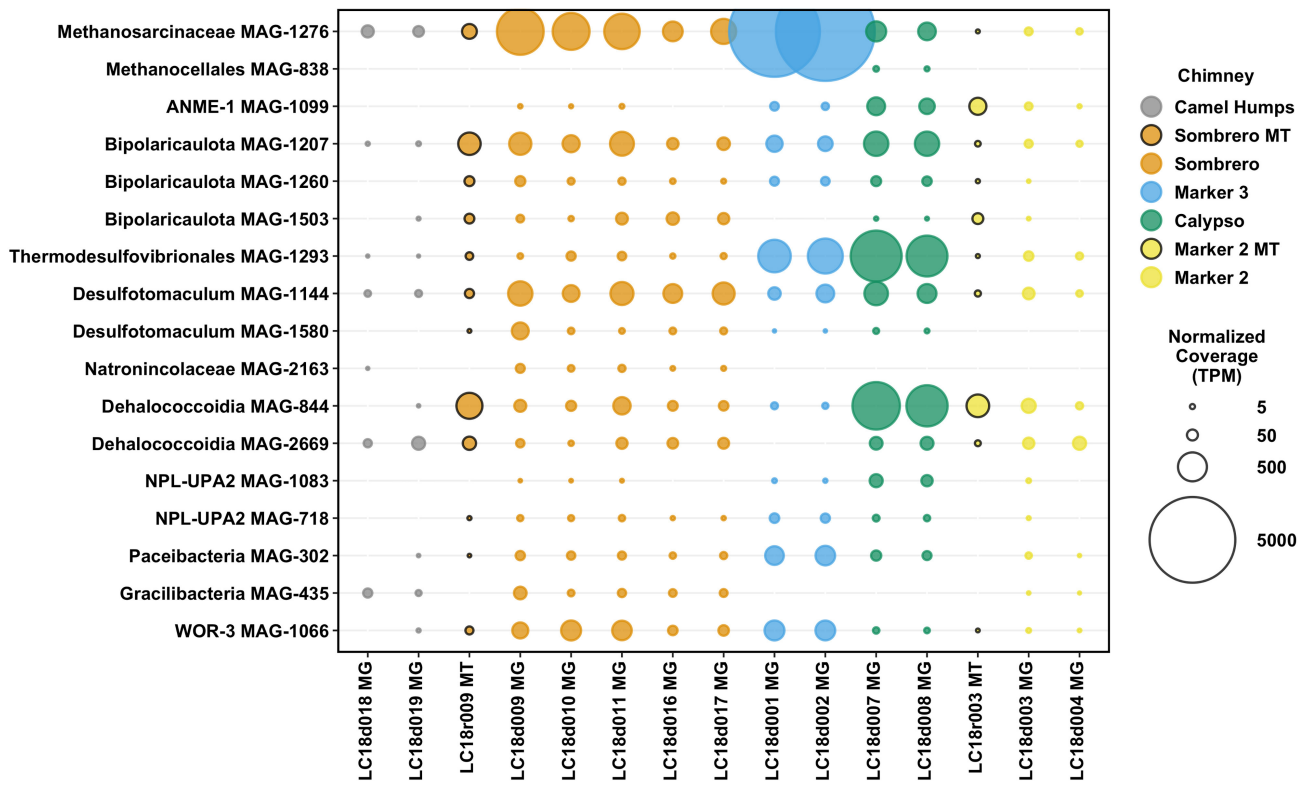


FIG 3 Abundance of refined MAGs in Lost City hydrothermal fluid samples. Total mapped read coverage was normalized to genome size and to the size of the metagenome or metatranscriptome library. The final normalized coverage is reported as a proportional unit (transcripts/fragments per million; TPM) suitable for cross-sample comparisons. Bubbles representing coverage in metatranscriptomes (MT), rather than metagenomes (MG), are highlighted with black borders. For clarity, not all MAGs are shown. A full coverage table is provided in Table S4.

Hydrogenases. [NiFe]-hydrogenases were found in *Thermodesulfobacteriales* MAG-1293 (HyaAB), *Methanocellales* MAG-838 (HyaAB), and *Bipolaricauota* MAG-1503 (HoxYH) (Fig. 4). Of these, the *Thermodesulfobacteriales* MAG was by far the most abundant in venting fluids (Fig. 3). *Methanosarcinaceae* MAG-1276 encodes two hydrogenases associated with methanogenesis: F₄₂₀-reducing hydrogenase (FrhAB) and the small and large subunits of a second hydrogenase predicted to be EchCE by GhostKOALA and group 4e hydrogenase (ferredoxin-coupled, Ech-type) by HydDB. The two hydrogenase subunits are encoded on a contig that includes six subunits of a H⁺:Na⁺ antiporter. The MAG also encodes a formate dehydrogenase that can provide electrons to MvhD and HdrABC instead of the H₂-oxidizing Vho/Vht enzyme (23). Thus, Lost City *Methanosarcinaceae* may power methanogenesis with electrons from both H₂ and formate. The same MvhD-HdrABC complex, without FDH, was also found in MAGs classified as ANME-1, *Natronincolaceae*, and *Bipolaricauota* (Table S5).

In addition, the *Methanosarcinaceae* and ANME-1 MAGs contain a complete 14-gene cluster (mbhA-N) encoding membrane-bound hydrogenase (Mbh) (Fig. 5; Fig. S8). For each predicted gene in the cluster, the homologs in the *Methanosarcinaceae* and ANME-1 MAGs are more similar to each other than to any other sequences in public databases. The same gene cluster, with conserved synteny, is also found in methanogens belonging to the order *Methanomicrobiales* and in heterotrophs of the order *Thermococcales* (24). The MbhL subunits from these methanogens have only 42% to 45% identities with the Lost City MbhL sequences reported here, which have greater similarity (~49% identities) to MbhL sequences from *Thermococcus*. *Bipolaricauota* MAG-1503 also includes a predicted MbhL sequence, which is most closely related to two *Bipolaricauota* MAGs from hydrothermal systems: the Mid-Cayman Rise (25) and Guaymas Basin (26) (Fig. 5).

[NiFe]-hydrogenase sequences (HyaAB) were also highly abundant in Sombrero and Camel Humps fluids (Table S7), where they were primarily encoded by *Thiomicrosrhabdus*.

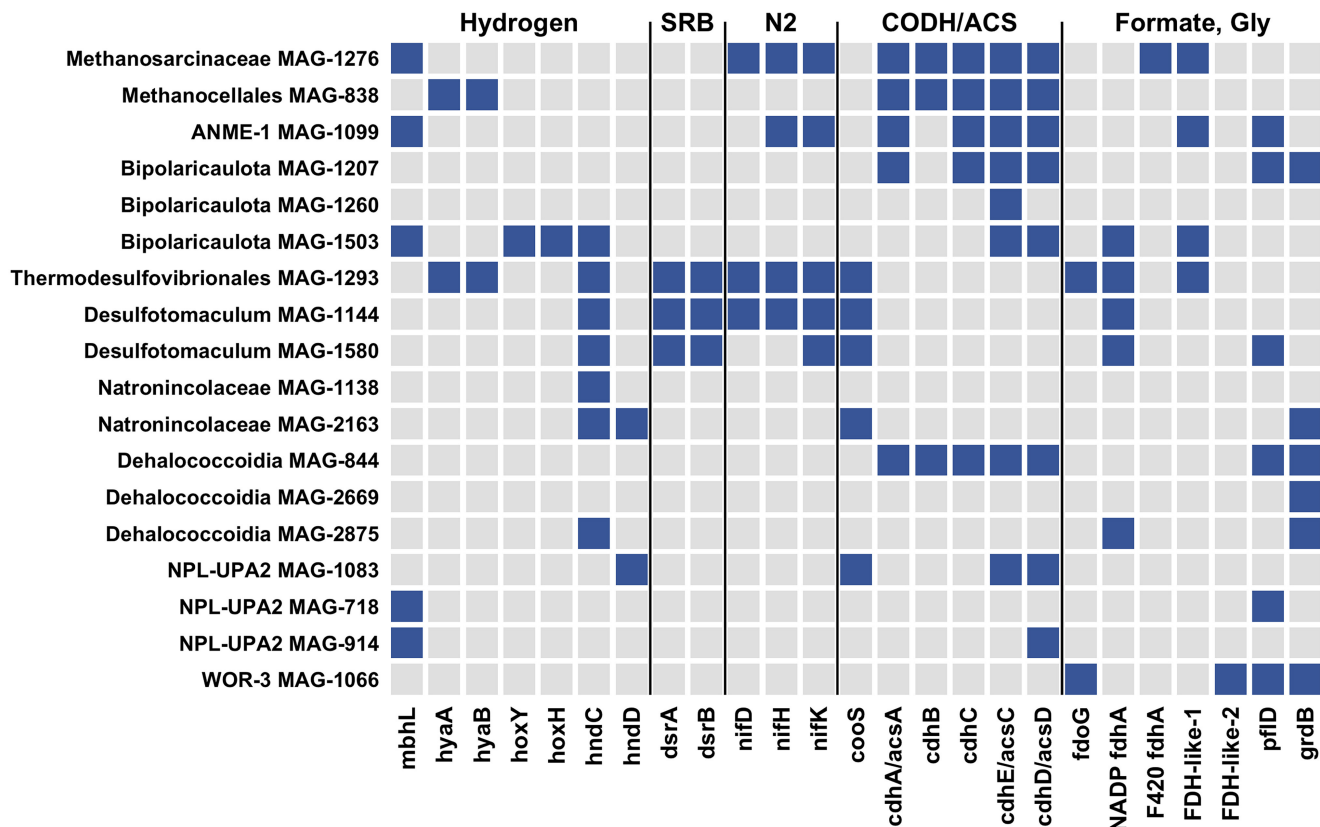


FIG 4 Presence and absence of key genes in refined MAGs. Genes defined by KEGG Orthology (see Table S5) were selected to highlight potential metabolic capabilities to metabolize hydrogen gas, to reduce sulfate to sulfide (SRB), to fix nitrogen (N_2) gas, to fix carbon dioxide via the Wood-Ljungdahl pathway (CODH/ACS), and to utilize formate or glycine as carbon sources. Patescibacteria MAGs (including Paceibacteria and Gracilibacteria) are not shown here because they lack all of the gene shown here.

We did not prioritize the analysis of *Thiomicrorhabdus* MAGs because our prior work indicated they inhabit oxygenated biofilm communities on chimney surfaces (27). We previously noted the absence of hydrogenase sequences phylogenetically linked with these bacteria (28), but recent sequencing of additional genomes from *Thiomicrospira*, *Thiomicrorhabdus*, and *Hydrogenovibrio* (29) has revealed many of the hydrogenase sequences in Lost City metagenomes are affiliated with these taxa after all.

[FeFe]-hydrogenases typically associated with the production of H_2 during fermentation were represented by HndCD sequences in one *Natronincolaceae* and one NPL-UPA2 MAG (Fig. 4). This hydrogenase is also capable of H_2 oxidation with reduction of NADP in some organisms (30). Therefore, the metabolic role of this hydrogenase in Lost City cannot be predicted with certainty.

Formate dehydrogenase and transporters. Formate dehydrogenase (FDH) catalyzes the reversible oxidation of formate to carbon dioxide, and various forms of FDH have diverse physiological roles in all three domains of life (31). Oxidation of formate was detected in shipboard incubations with ^{13}C -labeled formate with all Lost City fluid samples, including those with significant contributions from ambient seawater (Table S8). However, none of the incubations supplemented with ^{13}C -enriched formate or dissolved inorganic carbon (DIC) produced methane with a $\delta^{13}C$ that was distinguishable from that of methane native to Lost City fluids (approximately -10‰) (6, 11). Therefore, we conclude no methane was produced from DIC or formate during the seafloor incubations.

We identified at least three kinds of FDH in Lost City fluids plus two distinct variants of FDH-like sequences: (i) NAD(P)-dependent FDH catalyzing formate oxidation in bacteria (K00123; FdoG/FdhF/FdwA) was detected in *Thermodesulfovibrionales* and WOR-3 MAGs;

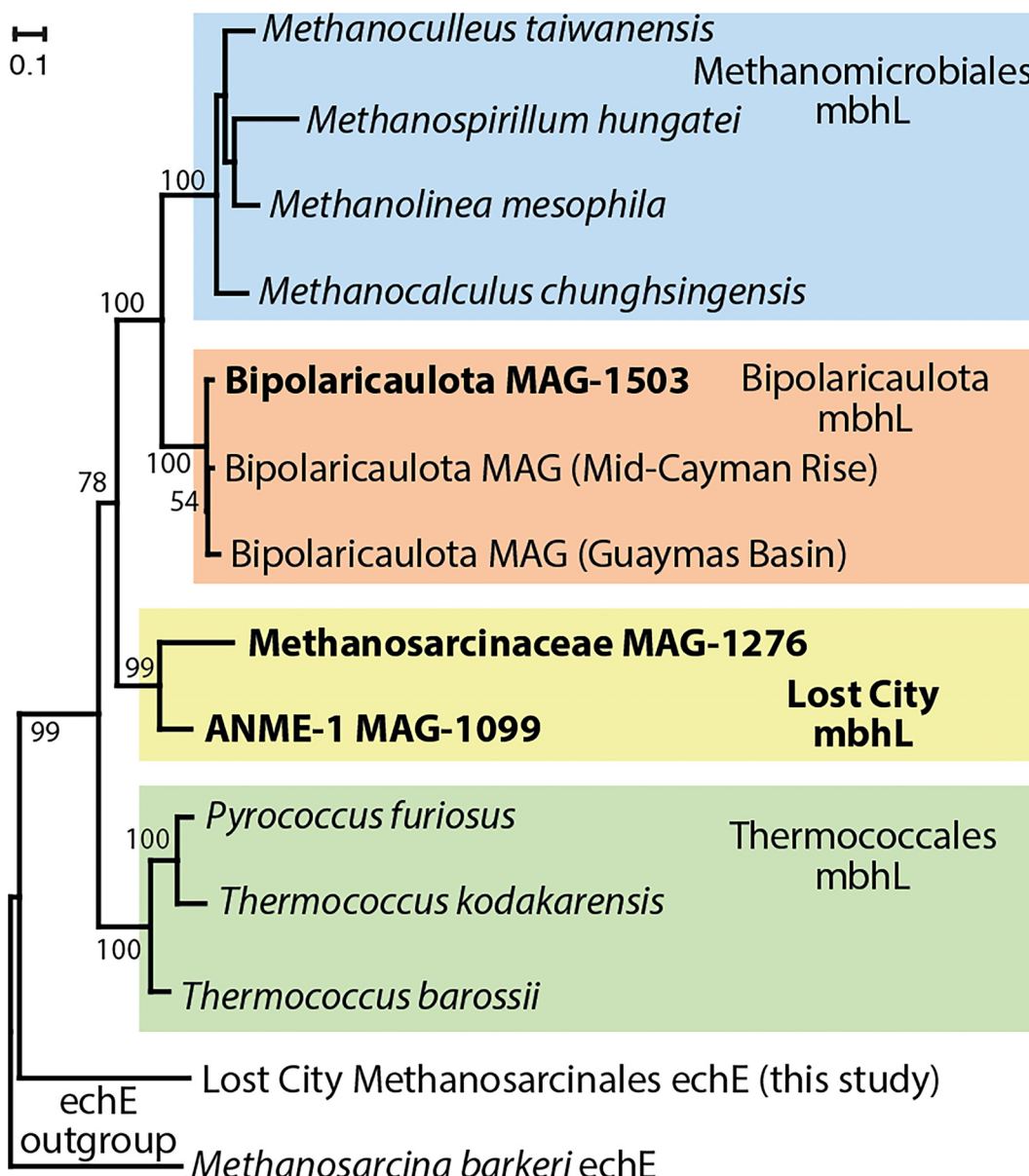


FIG 5 Phylogeny of the large catalytic subunit of membrane-bound hydrogenase (mbhL). Sequences identified in refined MAGs from this study are highlighted in bold font. The two archaeal sequences from Lost City (*Methanosarcinaceae* and ANME-1) form their own clade apart from all known mbhL sequences. The mbhL sequence from a Lost City Bipolaricaulota MAG clusters together with Bipolaricaulota MAGs from other hydrothermal environments. Bootstrap support values are shown for each node. An expanded version of this figure, including the gene order for the mbh gene cluster is provided as Fig. S8.

(ii) NAD(P)-dependent FDH catalyzing reduction of carbon dioxide into formate (K05299; FdhA) was detected in Bipolaricaulota, *Thermodesulfovibrionales*, *Desulfotomaculum*, and *Dehalococcoidia* MAGs; (iii) F₄₂₀-dependent FDH catalyzing formate oxidation in methanogens (K22516; FdhA) was detected in the *Methanosarcinaceae* MAG; (iv) a divergent FDH-like sequence was detected in *Methanosarcinaceae*, ANME-1, Bipolaricaulota, and *Thermodesulfovibrionales* MAGs; (v) another divergent FDH-like sequence, distinct from those described above such that it could not be reliably placed in the phylogeny of Fig. 6, was detected in the WOR-3 MAG (Fig. 4).

The divergent FDH-like sequence shared by the *Methanosarcinaceae*, ANME-1, Bipolaricaulota, and *Thermodesulfovibrionales* MAGs was identified by conducting blastp searches of the NCBI nr and JGI IMG databases for FDH homologs. Apparent homologs

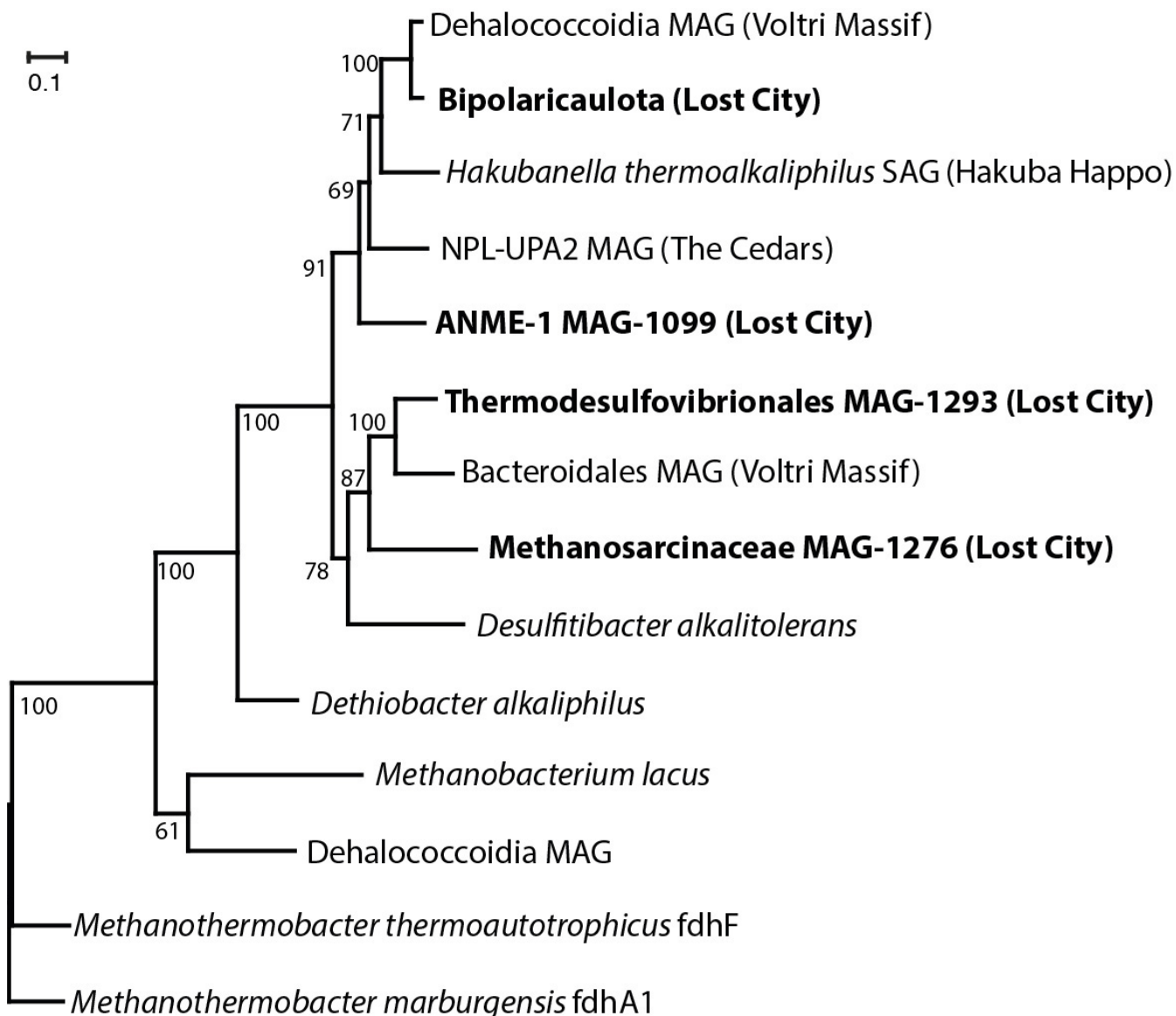


FIG 6 Phylogeny of divergent FDH-like sequences. Sequences identified in refined MAGs from this study are highlighted in bold font. Their closest matches in the NCBI nr database are from other serpentinite-hosted springs (Voltri Massif, Hakuba Happo, and The Cedars). The FDH-like sequences shown here include an iron-sulfur binding domain and a molybdopterin oxidoreductase domain, which are encoded as two separate coding regions in some species and as a fused coding region in others (see Fig. S9 an expanded version of this figure, including genomic context). The phylogeny was constructed from the conserved oxidoreductase domain. Bootstrap support values are shown for each node. The Lost City Bipolaricauota sequence was identified in multiple BinSanity bins classified as Bipolaricauota, but it was not included in the final, manually refined MAGs.

of these FDH-like sequences were also found in MAGs and SAGs (single-amplified genomes) from three continental serpentinite-hosted springs: the Voltri Massif in Italy (32), The Cedars in California, USA (33), and Hakuba Happo hot springs in Japan (34) (Fig. 6; Fig. S9). The serpentinization-associated FDH-like sequences share 65% to 94% amino acid identities with each other and approximately 40% to 50% amino acid identities with FDH sequences from characterized organisms, with the exception of *Desulfitibacter alkalitolerans* (63% amino acid identities). In a previous study, we reported these divergent FDH-like sequences as bacterial based on their similarity to *Desulfitibacter* sequences (10). Although *Desulfitibacter alkalitolerans* can use formate as an electron donor, it encodes two additional homologs of fdhA that are not present in any Lost City metagenomes. A similar FDH-like sequence is encoded by *Dethiobacter alkaliphilus*, which is unable to grow on formate as its sole carbon source (35). The phylogeny in Fig. 5 is rooted with FdhF (anaerobic formate hydrogen lyase) from *Methanothermobacter*

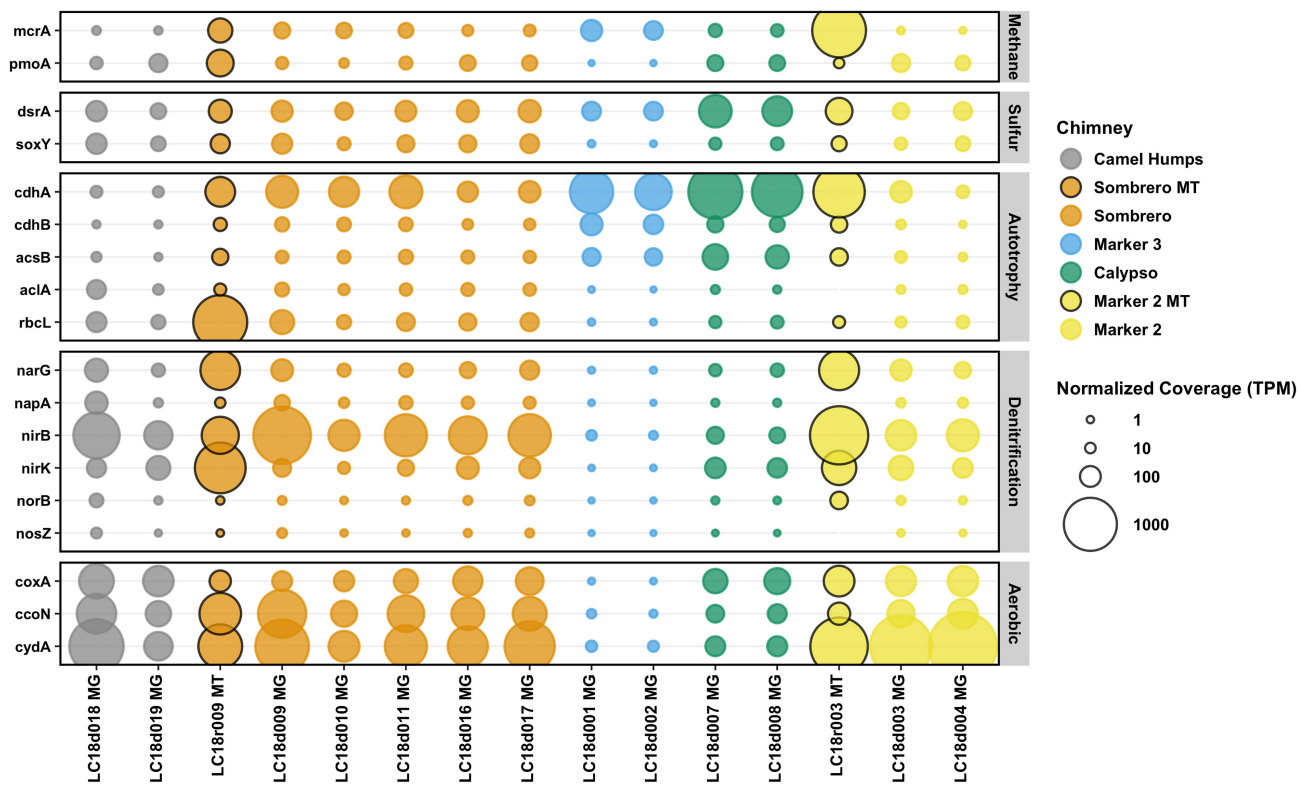


FIG 7 Abundance of key genes in Lost City hydrothermal fluid samples. Metagenomic coverage was normalized to predicted protein length and to the size of the metagenome or metatranscriptome library. The final normalized coverage is reported as a proportional unit (transcripts/fragments per million; TPM) suitable for cross-sample comparisons. Bubbles representing coverage in metatranscriptomes (MT), rather than metagenomes (MG), are highlighted with black borders. Genes are defined with KEGG Orthology; see Table S5.

thermautotrophicus and *Methanothermobacter marburgensis*. These two species are unable to grow on formate (36), and lack a separate fdhABC operon that is found in *M. thermautotrophicus* st. CaT2, which can grow on formate.

The formate transporters FdhC and FocA that were previously identified in Lost City chimney biofilms (10, 13) were also detected in the metagenomes of venting fluids reported here, but they were only present at very low coverage (Table S7). None of the MAGs highlighted by this study contain any known formate transporters. A lack of canonical formate transporters was also reported recently for a formate-utilizing methanogen in serpentinite-hosted, hyperalkaline groundwaters (37). Therefore, transport of formate into the cells of organisms inhabiting hyperalkaline subsurface environments may be carried out by uncharacterized proteins.

Sulfate reduction. Surprisingly, the samples of sulfidic fluids collected from the chimney at marker 2 (Table 1) did not contain elevated levels of taxa expected to represent SRB (Fig. 2 and 3) or the genes encoding dissimilatory sulfite reductase (DsrAB) (Fig. 7). Instead, marker 2 fluids are dominated by aerobic bacteria that are likely to be adapted to chimney biofilms or to shallow subsurface zones with exposure to ambient seawater. Potential SRB such as *Thermodesulfovibionales* were most abundant in the fluids venting from marker 3, marker C, Sombrero, and Calypso (Fig. 2 and 3).

The other potential SRB in Lost City fluids include *Desulfotomaculum*, *Desulfocapsa*, and *Desulfobulbus*. *Desulfotomaculum* have been implicated as potential SRB in Lost City chimney biofilms (38), but sequences predicted to encode hydrogenases or carbon fixation enzymes were not identified in the *Desulfotomaculum* MAGs; therefore, their ability to reduce sulfate may depend on the availability of organic matter. Furthermore, some *Desulfotomaculum* species are known to be incapable of sulfate reduction despite encoding DsrAB (39). *Desulfobulbus* sequences were very rare in fluids from markers 3

and *C. Desulfocapsa* were moderately abundant in marker 3 fluids, but no MAGs classified as *Desulfocapsa* could be recovered during this study. Additionally, most of the dsrAB sequences in Lost City fluids were affiliated with *Thermodesulfovibrionales* or *Desulfotomaculum*; no dsrAB sequences belonging to *Desulfocapsa* or *Desulfobulbus* were identified in high-coverage contigs.

Methane oxidation. Methane is present in Lost City fluids at a remarkably constant concentration of ~1 mM, while concentrations of H₂, sulfate, sulfide, and other chemicals vary widely (6, 9, 40). The source of the methane, i.e., whether it is synthesized abiotically as a product of serpentinization or released from carbon stored within basement rocks, remains uncertain (41–44). Oxidation of ¹³C-enriched methane to DIC with δ ¹³C values significantly greater than that of DIC native to Lost City fluids (<1.5 ‰) (6, 11) was detected in most Lost City fluid samples, except the sample of marker 3 fluids (Table S8).

The primary candidates for the anaerobic oxidation of methane at Lost City are the ANME-1 archaea, which are most abundant in Calypso fluids (Fig. 2 and 3). The Lost City ANME-1 MAG contains the core methanogenic pathway (Table S5), including F₄₂₀⁻ dependent methylenetetrahydromethanopterin reductase (Mer). This gene is required for methanogenesis from carbon dioxide, but it is typically absent in ANME genomes, with at least one exception previously reported (45). The MAG lacks all but one of the subunits of N⁵-methyl-H₄MPT:coenzyme M methyltransferase (Mtr), which catalyzes the penultimate step of methanogenesis (and putatively the second step of reverse methanogenesis). It is present in most but not all ANME-1 genomes (46). The absence of cytochromes and presence of hydrogenases in the ANME-1 MAG was noted by Chadwick et al. (46) as consistent with the genomic features of the so-called “freshwater” clade of ANME-1, for which the genus “*Candidatus Methanoalium*” was proposed. One of the shared features within this clade, including the Lost City ANME-1 MAG, is a novel HdrABC-MvhADG complex (46), which is involved in the transfer of electrons derived from H₂ to heterodisulfide and ferredoxin in methanogens. Therefore, this clade of ANME-1 may be involved in the H₂-fueled production of methane instead of, or in addition to, the oxidation of methane. Distinguishing between methanogenesis and the anaerobic oxidation of methane with genomic data alone is notoriously difficult (46), and the *Methanosarcinaceae* and ANME-1 MAGs reported here contain features that are potentially consistent with both the production and oxidation of methane.

Potential methanotrophic bacteria were represented by ASVs classified as the gammaproteobacterial family *Methylomonaceae* (e.g., *Methylobacterium*), but they are expected to represent chimney biofilm communities (15) and were not abundant in any of the fluids included in this study. ASVs classified as *Methyoceanibacter*, various species of which can aerobically oxidize methane, methanol, or other methylated compounds (47), were prominent in marker C fluids and very rare or absent in all other fluids (Table S2).

Carbonic anhydrase. At the high pH conditions of Lost City fluids, dissolved bicarbonate and carbonate are more stable than carbon dioxide, and the potential use of bicarbonate or carbonate as carbon sources has been explored in studies of continental sites of serpentinization (37, 48–52). Carbonic anhydrase catalyzes the reversible conversion between bicarbonate and carbon dioxide, which may enable cells to utilize bicarbonate obtained from the environment. *Methanosarcinaceae* MAG-1276 encodes a carbonic anhydrase that shares 59% to 85% amino acid identities with sequences found in three other MAGs from Lost City (classified as NPL-UPA2 and Bipolaricauota) and in one MAG from the Hakuba Happo hot spring (53). These novel carbonic anhydrase sequences share only 35% to 41% amino acid identities with previously characterized proteins, e.g., the beta class carbonic anhydrases from *Clostridium aceticum* (Fig. S10). The Lost City carbonic anhydrase sequences retain each of the conserved residues highlighted by Smith and Ferry (54) for beta class carbonic anhydrases. In addition, the *Methanosarcinaceae* MAG includes a predicted high-affinity bicarbonate transporter (SbtA).

Glycine reductase. Glycine may be generated abiotically in high-H₂ conditions or released as a primary thermogenic degradation production of biomass (55–58). The reduction of glycine to acetyl-phosphate is catalyzed by glycine reductase, which has been identified in metagenomes from multiple serpentinite-hosted springs (53). Seven of the Lost City MAGs encode glycine reductase, and in most of these genomes, glycine reductase (GrdEBCA) is in a gene cluster that includes selenium transferase (SelA), selenocysteine-specific elongation factor (SelB), and thioredoxin (TrxA) (Table S5), consistent with the gene organization of bacteria that conserve energy by reduction of glycine (59). Each of these MAGs also encodes a partial Wood-Ljungdahl pathway, including the key steps (formate-THF ligase and methenyl-THF cyclohydrolase dehydrogenase) that could potentially feed into the glycine reductase complex and thereby enable carbon fixation via the reductive glycine pathway (60). These initial observations remain to be verified with more complete genomic and experimental analyses but are consistent with early results from other serpentinization-associated environments (53).

ATP synthase. The production of ATP is catalyzed by the enzyme ATP synthase, which diverged into distinct archaeal and bacterial versions early in the evolution of life (61). A few of the bacterial MAGs in this study encode the archaeal form of ATP synthase (A-type or V-type) instead of the bacterial form (F-type). These include *Dehalococcoidia* MAG-844, Paceibacteria MAG-855, WOR-3 MAG-1066, and all three NPL-UPA2 MAGs (Table S5). Chloroflexi, Paceibacteria (previously named candidate phylum OD1), and NPL-UPA2 bacteria have also been observed to encode A-type ATP synthase in The Cedars, a continental serpentinite spring (33, 49). In addition, ATP synthase was completely absent in three of the Paceibacteria MAGs, as was the case for multiple Paceibacteria MAGs from The Cedars (49). *Natronincolaceae* MAG-1138 also lacks any ATP synthase genes, and its genomic content suggests an obligate fermentative lifestyle (supplemental material). Other genera within family *Natronincolaceae* include *Alkaliphilus* and *Serpentinicella*, which have been isolated from the Prony Bay hydrothermal field, which is also associated with serpentinization (62, 63).

DISCUSSION

Distinct zones of microbial activity in Lost City's basement. The massive edifice of Poseidon towers 60 m above the center of the Lost City hydrothermal field (Fig. 1). Alkaline hydrothermal fluids flow from the serpentinite basement and throughout the Poseidon structure, exiting at multiple locations across the field. The differing flow paths that lead to each location have distinct residence times (64) and produce distinct chemical and microbiological compositions of the venting fluids (9, 10, 18, 40).

For example, the venting locations marker 3 and Camel Humps sit only a few meters from each other at the summit of Poseidon, but the fluids venting from each structure appear to have taken different paths, which is reflected in their distinct microbial communities. Marker 3 fluids are dominated by a few archaeal and bacterial species that have the genomic potential to metabolize H₂, formate, and sulfate. Genes encoding methanogenesis, sulfate reduction, and carbon fixation pathways are much more abundant in marker 3 fluids than genes encoding aerobic respiration pathways (Fig. 7; Fig. S12 to 15). In contrast, Camel Humps fluids host a diverse assemblage of bacteria capable of using oxygen, nitrate, and nitrite as oxidants. These taxonomic and metabolic patterns are generally similar between ribosomal gene and rRNA data sets (Fig. 2) and between metagenomes and metatranscriptomes (Fig. 3 and 7) from the same locations, indicating that the most abundant organisms in these fluids were likely to have been metabolically active at the time of sampling.

Sulfate reduction is limited to a few taxa in the subseafloor. Previous studies of Lost City hydrothermal fluids have revealed a consistent trend across the field in which the consumption of H₂ and sulfate is correlated with the production of hydrogen sulfide (9–11). Therefore, SRB are expected to be widespread and metabolically active in the subsurface environments below the Lost City chimneys.

The metagenomic results presented here indicate a single, novel species of *Thermodesulfovibronales* as the SRB that is most likely to be responsible for these

trends. It dominates the fluids at marker C, marker 3, and Calypso, and accounts for most of the genes associated with sulfate reduction and H₂ oxidation in these fluids. It also includes multiple formate dehydrogenases and various genes indicative of organic carbon oxidation (Table S5), suggesting metabolic flexibility that is not dependent on the availability of H₂ and inorganic carbon.

The Lost City *Thermodesulfovibrionales* belong to a novel clade associated with deep subsurface environments and hot springs that shares only 82% to 87% nucleotide identities with the 16S rRNA genes of characterized *Thermodesulfovibrio* species (Fig. S7). Members of this clade of *Thermodesulfovibrionales* are also abundant and potentially important sulfate-reducing bacteria in chimneys of the "Old City" hydrothermal field along the Southwest Indian Ridge (22) and in highly alkaline borehole fluids associated with serpentinization of the Samail Ophiolite in Oman (5, 65, 66). In addition, sequences classified as *Thermodesulfovibrionales* (or at least the parent phylum *Nitrospirota*) have been detected in chimneys of the Prony Bay hydrothermal field (21), alkaline borehole fluids from the Coast Range Ophiolite (67), natural springs associated with the Zambales Ophiolite in the Philippines (68), and in the Hakuba Happo hot springs (34), but these short 16S rRNA sequences were generally found at low relative abundances and have not been compared with other *Thermodesulfovibrionales* in any phylogenetic analyses. Sulfate concentrations are much higher in borehole fluids from the Samail Ophiolite (up to 3.9 mM) and the Coast Range Ophiolite (up to 0.4 mM) compared with most natural springs associated with serpentinization (e.g., <0.02 mM in the Tablelands, Voltri Massif, and The Cedars) (32, 65, 67, 69). An exception is Ney Springs, where sulfate can be as high as 12.9 mM, but the potential SRB detected there did not include *Thermodesulfovibrionales* (70). In summary, this clade of *Thermodesulfovibrionales* is most abundant in marine sites of serpentinization (e.g., chimneys of Lost City and Old City) and in continental sites of serpentinization with elevated concentrations of sulfate (e.g., boreholes in Samail and Coast Range ophiolites).

H₂-fueled metabolism is limited to a few taxa in the subseafloor. Lost City fluids contain copious quantities of H₂ (1 to 7 mM, with subsurface concentrations predicted to reach 14 mM) (6, 40), which is expected to be a tremendous boost to life in the subseafloor. Surprisingly, only two taxa (*Thermodesulfovibrionales* and *Methanosaerincaceae*) that are abundant in Lost City fluids encode hydrogenases known to be associated with hydrogenotrophy. Therefore, the ability of the subseafloor ecosystem to be powered by H₂ may depend on one species of bacteria and one species of archaea.

Another type of hydrogenase, known as membrane-bound hydrogenase (Mbh), was also detected in *Methanosaerincaceae*, ANME-1, and Bipolaricauota genomes (Fig. 5). In *Thermococcus* and *Pyrococcus*, Mbh is responsible for H₂ production during anaerobic, heterotrophic growth, and some bacteria use Mbh in coordination with FDH to convert formate into H₂ (71, 72). In heterotrophic Bipolaricauota, Mbh has been proposed to couple the production of H₂ with ATP synthesis in coordination with the MvhAGD-HdrABC complex (73). In methanogens, the role of Mbh is unclear, but each of the methanogens that encode Mbh can utilize either formate or H₂ as their sole source of electrons. Mbh has also been identified in a formate-consuming methanogen from the Samail Ophiolite, where it is proposed to be involved in the oxidation or reduction of ferredoxin (37). In H₂-saturated Lost City fluids, biological production of additional H₂ seems highly unfavorable, and the sequence divergence between the Lost City sequences and these previously characterized Mbh prevents any firm conclusions on whether they are more likely to catalyze the consumption or production of H₂. Future metagenomic studies of other environments where these clades of *Methanosaerincaceae*, ANME-1, and Bipolaricauota occur (21, 22, 49) would help to test whether these genes are uniquely adapted to the conditions of serpentinizing environments.

Formate metabolism may operate via unknown mechanisms in the subseafloor. Formate forms abiotically in the high-pH, reducing conditions of serpentinizing fluids, and is the second-most abundant form of carbon in Lost City fluids after methane and the second-most available reductant after dissolved H₂ (4). Much of the biomass in Lost City chimneys is derived from carbon that originated in Earth's mantle (9),

most likely in the form of formate (10). Formate is the preferred substrate for methanogens in at least one other site of serpentinization where carbon dioxide is limiting (37). However, none of the taxa highlighted by this study contain any known formate transporters, and surprisingly few encode formate dehydrogenase (FDH), the enzyme that catalyzes the oxidation of formate. A remarkable exception is *Thermodesulfovibrionales*, which encodes three distinct forms of FDH.

A divergent, FDH-like sequence with unknown function was shared by four of the key taxa in this study (*Thermodesulfovibrionales*, *Methanosarcinaceae*, ANME-1, and *Bipolaricaulota*). These sequences form a distinct clade that includes sequences from continental serpentinite springs, suggesting this gene represents a shared, unknown metabolic strategy in serpentinizing fluids (Fig. 6). At present, this phylogeny is sparse and lacks representatives of *Thermodesulfovibrionales* and *Methanosarcinaceae* from other sites of serpentinization where those taxa are abundant (5, 21, 22, 74). For example, no *Methanosarcinaceae* MAGs from other serpentinizing environments have yet been reported. Therefore, ongoing and future metagenomic studies of these environments will soon reveal whether the divergent form of FDH reported here is widespread among taxa and environments associated with serpentinization.

In the highly reducing conditions of Lost City fluids, biosynthetic pathways are more energetically favorable than in typical environments, and the synthesis of some biomolecules can even be energy-yielding (58, 75). Therefore, the ability to incorporate formate directly into metabolic pathways, rather than first oxidizing it to carbon dioxide, could be a competitive advantage in Lost City's basement, where formate is 100 to 1,000 times more abundant than carbon dioxide (4). Potential evidence for this hypothesis is the prevalence of partial and complete Wood-Ljungdahl pathways among Lost City bacteria (Table S5). Eight of these genomes do not encode a known FDH, suggesting they may be able to use formate, rather than carbon dioxide, as the substrate for carbon fixation and perhaps acetogenesis. Some acetogens can use formate as their sole source of energy and carbon, although FDH may be still required to supply carbon dioxide as an electron acceptor (76).

In the absence of FDH, pyruvate formate lyase (PflD), which is encoded by some of the same genomes with partial Wood-Ljungdahl pathways (*Bipolaricaulota*, NPL-UPA2, and *Dehalococcoidia*), might catalyze the reduction of formate directly into acetyl-CoA and pyruvate (77). However, this activity has only been demonstrated in *Escherichia coli*, and its relevance to these taxa in the unusual environmental conditions of Lost City requires further research.

Conclusions. This study has highlighted multiple examples of metabolic strategies shared among the archaea and bacteria most likely to inhabit subsurface habitats underlying the Lost City hydrothermal field. These shared strategies appear to be advantageous for life in environments that are rich in H₂ (e.g., hydrogenases), provide a steady supply of simple organic molecules (e.g., formate dehydrogenase, pyruvate formate lyase, and glycine reductase), lack carbon dioxide (e.g., carbonic anhydrase), and make typical ATP synthesis too difficult or unnecessary (e.g., the absence of ATP synthase in some MAGs).

Many of the predicted proteins associated with these metabolic strategies are not closely related to any previously characterized enzymes, but are shared by diverse archaea and bacteria in Lost City and other sites of serpentinization (e.g., Old City, Prony Bay, The Cedars, Samail Ophiolite, Coast Range Ophiolite, Hakuba Happo, and Voltri Massif), strongly suggesting the influence of horizontal gene transfer among these systems. The functions of these proteins are mostly unknown and require further study, but the results presented here indicate they are likely to be important clues for understanding the ecology, physiology, and evolution of microbes adapted to these conditions.

If potential extraterrestrial habitats are evaluated for their ability to support a robust ecosystem over geological time scales (78), then it is critical to identify and understand the metabolic pathways of key organisms that form the foundations of ecosystems

that are potentially relevant for astrobiology. All ecosystems on the surface of the Earth are based on autotrophs that rely on the availability of sunlight and carbon dioxide. The most promising extraterrestrial habitats in our solar system (79–82), however, are dark, rock-hosted environments where simple organic molecules may be more biologically available than carbon dioxide. The organisms and metabolic pathways highlighted by this study can help us to understand the biological advantages and limitations of such conditions.

MATERIALS AND METHODS

Collection of hydrothermal fluid samples. Hydrothermal fluid samples were collected from actively venting chimneys at the Lost City hydrothermal field (Fig. 1) using ROV *Jason* during the 2018 Lost City expedition aboard R/V *Atlantis* (AT42-01). On the seafloor, venting fluids were slowly pumped through 0.2 μm Millipore Sterivex cartridge filters or into acid-washed Kynar bags with the HOG sampler (83). Samples intended for RNA extractions were collected into 2 L Kynar bags containing 67 mL of a stop solution (97.5% 200 proof ethanol, 2.5% TRIzol LS; Thermo Fisher). Fluid temperatures were monitored in real-time during sampling with a probe embedded into the sampler intake. Immediately upon shipboard recovery of ROV *Jason*, all Sterivex filters were stored at -80°C . Kynar bags were subsampled for shipboard aqueous chemistry measurements (pH, magnesium, sulfate, and hydrogen sulfide) according to standard methods (84) and filtered through Sterivex filters, which were subsequently frozen at -80°C . The estimated precision of the analyses is 3% for magnesium, 2% for sulfate, and 4% for hydrogen sulfide (all as relative standard deviation). All frozen filters were shipped overnight to the University of Utah on dry ice or in liquid nitrogen vapor shippers.

Cell counts. Aliquots of all fluid samples were preserved in 3.7% formaldehyde and stored at 4°C . In the Anderson lab (Carleton College), preserved fluids were filtered onto 0.22 μm black polycarbonate filters and stained with DAPI (85). Cells were enumerated directly with an epifluorescence microscope, and a minimum of 20 fields of view were counted per sample. The median number of cells per field of view was recorded as the result for that sample, and the median value among all replicates is reported as the value for each location in Table 1.

Bags supplemented with formate or methane. On each dive, some of the 2 L Kynar bags were supplemented with ^{13}C -enriched bicarbonate, formate, or methane (Cambridge Isotope Laboratories) to test for conversion of these compounds into DIC or methane inside the Kynar bags. Thus, these Kynar bags served as seafloor incubation experiments. In addition, each bag contained 0.2 g of dithiothreitol, intended as a redox buffer. Upon shipboard recovery, the bags were subsampled and processed for DNA sequencing as described above, and additional aliquots of the fluid sample were collected for analysis of ^{13}C enrichment of methane and DIC. In the Lang lab (University of South Carolina), the ratio of $^{13}\text{C}/^{12}\text{C}$ of headspace CO_2 was analyzed using a Thermo Scientific GasBench-Delta V Plus isotope ratio mass spectrometer (IRMS). The $^{13}\text{C}/^{12}\text{C}$ of CH_4 was analyzed with a Thermo Scientific Gas Chromatograph-IsolinkII-IRMS equipped with an Agilent GS - CarbonPlot column (30 m \times 0.320 mm i.d., 1.50 μm film thickness). Amplicon sequencing was conducted on each fluid sample separately, and no consistent differences in microbial community composition were detected among fluids collected in incubation bags compared with *in situ*-filtered Sterivex filters (Table S2). Nevertheless, separate metagenome libraries were constructed with DNA prepared from *in situ*-filtered Sterivex filters and from incubation bags (Table S1).

Analysis of 16S rRNA ASVs. Sequencing of amplicons generated from 16S rRNA genes and cDNA was performed at the Genomics Core Facility at Michigan State University on an Illumina MiSeq instrument using dual-indexed Illumina fusion primers targeting the V4 region of the 16S rRNA gene (86). ASVs were inferred from 16S rRNA amplicon sequences with DADA2 v. 1.10.1 (87) after removal of primer sequences with cutadapt v. 1.15 (88). Sequences from different sequencing runs were processed with DADA2 separately, and then the resulting ASVs from all sequencing runs were merged to form a final, nonredundant count table of ASVs. Potential contaminants were removed with the decontam package (89) using both the “frequency” and “prevalence” modes. In the “frequency” mode, ASVs were removed if their counts were significantly correlated ($P < 0.02$) with DNA concentration (as measured by Qubit fluorometric quantification, Thermo Fisher). In the “prevalence” mode, ASVs were removed if they were significantly more likely ($P < 0.02$) to be present in one of three likely contamination sources (ambient lab air, surface seawater, or DNA extraction blanks) than in any sample of hydrothermal fluid. Samples of ambient air in the R/V *Atlantis* shipboard laboratory and our laboratory at the University of Utah were obtained as previously described (14). Samples of surface seawater were obtained during a previous study at the same location above the Atlantis Massif (14) and also from the shipboard laboratory “tap” water produced from surface seawater by the R/V *Atlantis*. DNA extraction blanks were obtained by Motamedei et al. by subjecting sterile Sterivex filters to the DNA extraction protocol described above (14). All contamination control samples were sequenced on the same sequencing runs as described above for the hydrothermal fluid samples. A total of 1,823 ASVs (9% of all ASVs) representing 109,824 sequence counts (2% of all sequence counts) were removed from downstream analyses by decontam. These removed ASVs are provided in Table S2.

Taxonomic classification of all ASVs was performed with DADA2 using the SILVA reference alignment (SSURefv132) and taxonomy outline (90, 91). Bubble plots of ASVs were drawn with ggplot2 using proportional abundances. The ordination plot was generated with phyloseq v1.26.1 (92) using an unconstrained NMDS ordination of Morisita-Horn dissimilarity values. The stress of the fit to two dimensions

was 0.05 after 20 tries without a convergent solution. Very similar results were produced with MDS and CCA ordinations and with Bray-Curtis dissimilarity values.

Differential abundances of ASVs between the marker 3 and Camel Humps locations were calculated with DESeq2 (93) as implemented by phyloseq (92). ASVs with variance $<10^{-5}$ were filtered out prior to the test, and those ASVs with an adjusted P -value <0.05 were considered to be differentially abundant.

Sequencing of metagenome libraries. Metagenome libraries were constructed with size-selected, sonicated DNA fragments of 500 to 700 bp with the NEBnext Ultra DNA II library kit for Illumina (E7645S), as previously described (94). Paired-end sequencing (2×125 bp) of metagenomic libraries was conducted at the University of Utah High-Throughput Genomics Core Facility at the Huntsman Cancer Institute with an Illumina HiSeq 2500 platform. Sequencing libraries (25 pM) were chemically denatured and applied to an Illumina HiSeq v4 paired end flow cell using an Illumina cBot. Hybridized molecules were clonally amplified and annealed to sequencing primers with reagents from an Illumina HiSeq PE Cluster Kit v4-cBot. Following transfer of the flowcell to an Illumina HiSeq 2500 instrument (HCS v2.2.38 and RTA v1.18.61), a 125 cycle paired-end sequence run was performed using HiSeq SBS Kit v4 sequencing reagents (FC-401-4003).

Sequencing of metatranscriptome libraries. Only two samples (one from marker 2 and one from Sombrero) contained sufficient total RNA to attempt metatranscriptome sequencing. The two metatranscriptome libraries were constructed and sequenced by the University of Utah High-Throughput Genomics Core Facility at the Huntsman Cancer Institute. Total RNA was hybridized with NEBNext rRNA Depletion Solution Bacteria (E7850L) to substantially diminish rRNA from the samples. Stranded RNA sequencing libraries were prepared using the NEBNext Ultra II RNA Library Prep Kit for Illumina (E7770L). Purified libraries were qualified on an Agilent Technologies 2200 TapeStation using a D1000 ScreenTape assay. The molarity of adapter-modified molecules was defined by quantitative PCR using the Kapa Biosystems Kapa Library Quant Kit. Individual libraries were normalized to 10 nM, and equal volumes were pooled. Sequencing libraries were chemically denatured and applied to an Illumina NovaSeq flow cell using the NovaSeq XP workflow (20043131). Following the transfer of the flowcell to an Illumina NovaSeq 6000 instrument, a 150 cycle paired-end sequence run was performed using a NovaSeq 6000 S4 reagent kit v1.5 (20028312).

Quality control and taxonomic classification of metagenome and metatranscriptome sequences. Demultiplexing and conversion of the raw sequencing base-call data were performed through the CASAVA v1.8 pipeline. Adapter sequences and PhiX were removed from all reads with BBduk (part of the BBTools suite, v35.85 [95]). Quality trimming was performed with our seq-qc package (<https://github.com/Brazelton-Lab/seq-qc>) as previously described (94). Each library yielded 22 to 192 million reads (for a total of 1.4 billion reads among all metagenome libraries) after these quality control steps, representing 58% to 82% of the number of raw reads. The two metatranscriptome libraries yielded 249 million reads (marker 2) and 467 million reads (Sombrero) after quality filtering, representing 82% and 88%, respectively, of the original raw reads. rRNA sequences were identified in the two metatranscriptomes with SortMeRNA (96), resulting in the removal of 77% of reads from the marker 2 metatranscriptome and 90% of reads from the Sombrero metatranscriptome. Quality-filtered, unassembled reads were assigned taxonomy with Kaiju and the NCBI nr+euk database (97). Kaiju was unable to classify 46% to 86% of reads, with the lowest percentage of unclassified reads in metatranscriptomes and the highest percentage of unclassified reads in the two marker 3 metagenomes and one Sombrero metagenome (Table S3). An interactive Krona plot is provided in the Zenodo-archived GitHub repository (doi:10.5281/zenodo.5798015).

Metagenomic assembly. Sequences from metagenomic libraries were assembled with Megahit v1.1.1 (98), using kmers of 27 to 127. A pooled “all fluids” Megahit assembly was performed with metagenomic reads from all 13 libraries (representing 37 fluid samples collected in Sterivex filters and Kynar bags; see Table S1). Genes were predicted with Prodigal v2.6.3 (99) in meta mode. Predicted protein sequences were queried against the KEGG release 83.2 prokaryotes database with Diamond v0.9.14 (100).

In addition to the “all fluids” Megahit assembly, chimney-specific assemblies were conducted with metaSPAdes v3.13.0 (101) as implemented by the KBase platform (kb_SPAdes v.1.2.4) (102). A chimney-specific assembly with reads obtained from marker 3 was performed with Megahit v1.1.1 because metaSPAdes repeatedly failed when it attempted to assemble marker 3 reads. An overview of the metagenomic analysis workflow is illustrated in Fig. S3.

Binning of MAGs. Binning of MAGs from the “all fluids” and marker 3 Megahit assemblies was conducted with BinSanity using the Binsanity-lc workflow v0.2.6.2 and a minimum contig size of 3 kb (103). Binning of MAGs from the chimney-specific metaSPAdes assemblies was conducted with MaxBin2 v2.2.4 (kb_maxbin v.1.1.1) (104), MetaBAT2 v2.2 (kb_metabat v.2.3.0) (105), and DAS Tool v1.1.2 (kb_das_tool v.1.0.6) (106). The ANME-1 MAG was reconstructed from a Megahit assembly of Calypso reads with MetaBAT2 and DAS Tool. MAGs were assigned taxonomic classifications with GTDB-Tk v1.5.1 (reference data version r202; [107]). Individual contigs were assigned taxonomic classifications with MMseqs2 (108). Gene products were predicted by annotation with Prokka v1.14.5 and its default databases (109) with further function prediction provided by GhostKOALA v2.2 (110). Protein identifications and predicted functions were supplemented by results from InterProScan 5 (V5.52-86.0) (111), HydDB (112), FeGenie (113), and dbCAN2 (114). Completeness and contamination of initial automated MAGs were estimated with CheckM v1.0.5 (115), and the completeness and redundancy of the final refined MAGs were estimated with anvi'o v7 (116). Selected MAGs were refined by reassembly with metaSPAdes v3.11.1 using reads mapped to MAGs and contigs with matching taxonomic classifications, followed by manual curation in anvi'o v7 (117) according to the differential coverage of contigs among samples.

Coverages of genes, contigs, and MAGs. Quality-filtered metagenome and metatranscriptome sequences were mapped to the “all fluids” Megahit assembly with Bowtie2 v2.3.2 (118). Bowtie2 mapping rates to the “all fluids” assembly were 67% to 71% for Camel Humps, 82% to 89% for Sombrero1, 60% to 71% for Sombrero2, 95% for marker 3, 67% to 74% for Calypso, and 56% to 60% for marker 2. Bowtie2 mapping rates to the “all fluids” assembly were 21% before rRNA removal and 14% after rRNA removal for the marker 2 metatranscriptome and 83% before rRNA removal and 74% after rRNA removal for the Sombrero1 metatranscriptome. Artificial duplicates were removed from the bam files using the MarkDuplicates function of Picard Tools v2.17.8 (119).

The coverage for each predicted protein was calculated as TPM with count_features v1.3.0, part of our seq-annot package (94). TPM is a proportional unit (multiplied by one million for convenience) that is normalized to the length of each predicted protein sequence as well as to the total library size. Coverages of both metagenomes and metatranscriptomes were calculated in the same way and reported in the same units (TPM), although the metagenomic coverages reflect fragments instead of transcripts (94).

The coverage of each MAG was calculated as the weighted sum of the normalized, proportional coverages (in TPM) of its member contigs. The contig coverages were obtained by mapping all unassembled reads against the reassembled, refined MAGs with Bowtie2 and then calculating the average coverage per position of each contig with the genomecov command (with the option -pc) in bedtools v2.30.0 (120). Normalized coverages in units of TPM were calculated by dividing the average coverage per position by the total number of read pairs for that library.

Phylogenetic analyses. Phylogenetic trees of 16S rRNA genes were constructed with alignments obtained from the SILVA alignment server (121) and RAxML v8.2.11 (122) using the gamma model of rate heterogeneity and the “-f a” option to construct 100 rapid bootstrap searches and 20 maximum likelihood searches. The *Thermodesulfobacteriales* ASV from the Samail Ophiolite, Oman (65) was generated with DADA2 as described above with reads accessed via SRA accession [SRR5000240](#). Phylogenies of McrA, GrdB, and carbonic anhydrase were constructed with Clustal Omega alignments (123) and RAxML as described above but with automated selection of the rate model. All sequences and accessions are provided in the Zenodo-archived GitHub repository accessible via doi:[10.5281/zenodo.5798015](#).

Data availability. Amplicon sequences are available via NCBI BioProject [PRJNA672129](#), and metagenome and metatranscriptome sequences are available via BioProject [PRJNA779602](#). MAGs are associated with the same BioProject and are individually accessible via BioSamples [SAMN23474158](#) - [SAMN23474187](#). In addition, GenBank accessions are listed for each MAG in Table S4. Protocols, metadata, and additional data are provided in a Zenodo-archived GitHub repository accessible via doi:[10.5281/zenodo.5798015](#), and on the BCO-DMO page for project 658604: <https://www.bco-dmo.org/project/658604>.

SUPPLEMENTAL MATERIAL

Supplemental material is available online only.

SUPPLEMENTAL FILE 1, PDF file, 6.1 MB.

SUPPLEMENTAL FILE 2, XLSX file, 0.02 MB.

SUPPLEMENTAL FILE 3, XLSX file, 10.5 MB.

SUPPLEMENTAL FILE 4, XLSX file, 0.6 MB.

SUPPLEMENTAL FILE 5, XLSX file, 0.1 MB.

SUPPLEMENTAL FILE 6, XLSX file, 0.1 MB.

SUPPLEMENTAL FILE 7, XLSX file, 0.2 MB.

SUPPLEMENTAL FILE 8, XLSX file, 2.6 MB.

SUPPLEMENTAL FILE 9, XLSX file, 0.01 MB.

ACKNOWLEDGMENTS

We thank the Scientific Party of the 2018 Lost City expedition (AT42-01), including the crews of R/V *Atlantis* and ROV *Jason*. In addition, we gratefully acknowledge invaluable mentorship for many years from John Baross and Deborah Kelley. Mitch Elend, Christopher Thornton, and Alex Hyer provided critical technical support before, during, and after the expedition. University of Utah students enrolled in BIOL 3270/5270 assisted in the analysis of metagenomic data.

This work was supported by NSF awards to W.J.B. and S.Q.L. (OCE-1536702/1536405), the NASA Astrobiology Institute Rock-Powered Life team, a NASA Postdoctoral fellowship to J.M.M., the Swiss National Science Foundation, and the Deep Carbon Observatory.

REFERENCES

- McCollom TM, Seewald JS. 2007. Abiotic synthesis of organic compounds in deep-sea hydrothermal environments. *Chem Rev* 107:382–401. <https://doi.org/10.1021/cr0503660>.
- Martin W, Baross J, Kelley D, Russell MJ. 2008. Hydrothermal vents and the origin of life. *Nat Rev Microbiol* 6:805–814. <https://doi.org/10.1038/nrmicro1991>.

3. Schrenk MO, Brazelton WJ, Lang SQ. 2013. Serpentinitization, carbon, and deep life. *Rev in Mineralogy and Geochemistry* 75:575–606. <https://doi.org/10.2138/rmg.2013.75.18>.
4. Lang SQ, Brazelton WJ. 2020. Habitability of the marine serpentinite subsurface: a case study of the Lost City hydrothermal field. *Philos Trans A Math Phys Eng Sci* 378:20180429. <https://doi.org/10.1098/rsta.2018.0429>.
5. Templeton AS, Ellison ET, Glombitzka C, Morono Y, Rempfert KR, Hoehler TM, Zeigler SD, Kraus EA, Spear JR, Nothaft DB, Fones EM, Boyd ES, Munro-Ehrlich M, Mayhew LE, Cardace D, Matter JM, Kelemen PB, the ODPS party. 2021. Accessing the subsurface biosphere within rocks undergoing active low-temperature serpentinization in the Samail Ophiolite (Oman Drilling Project). *J Geophys Res Biogeosci* 126. <https://doi.org/10.1029/2021JG006315>.
6. Kelley DS, Karson JA, Früh-Green GL, Yoerger DR, Shank TM, Butterfield DA, Hayes JM, Schrenk MO, Olson EJ, Proskurowski G, Jakuba M, Bradley A, Larson B, Ludwig K, Glickson D, Buckman K, Bradley AS, Brazelton WJ, Roe K, Elend MJ, Delacour A, Bernasconi SM, Lilley MD, Baross JA, Summons RE, Sylva SP. 2005. A serpentinite-hosted ecosystem: the Lost City hydrothermal field. *Science* 307:1428–1434. <https://doi.org/10.1126/science.1102556>.
7. Karson JA, Früh-Green GL, Kelley DS, Williams EA, Yoerger DR, Jakuba M. 2006. Detachment shear zone of the Atlantis Massif core complex, Mid-Atlantic Ridge, 30°N. *Geochem Geophys Geosyst* 7:n/a-n/a. <https://doi.org/10.1029/2005GC001109>.
8. Früh-Green GL, Orcutt BN, Rouméon S, Lilley MD, Morono Y, Cotterill C, Green S, Escartin J, John BE, McCaig AM, Cannat M, Ménez B, Schwarzenbach EM, Williams MJ, Morgan S, Lang SQ, Schrenk MO, Brazelton WJ, Akizawa N, Boschi C, Dunkel KG, Quéméneur M, Whattam SA, Mayhew L, Harris M, Bayrakci G, Behrmann J-H, Herrero-Bervera E, Hesse K, Liu H-Q, Ratnayake AS, Twing K, Weis D, Zhao R, Bilenker L. 2018. Magmatism, serpentinization and life: insights through drilling the Atlantis Massif (IODP Expedition 357). *Lithos* 323:137–155. <https://doi.org/10.1016/j.lithos.2018.09.012>.
9. Lang SQ, Früh-Green GL, Bernasconi SM, Lilley MD, Proskurowski G, Méhay S, Butterfield DA. 2012. Microbial utilization of abiogenic carbon and hydrogen in a serpentinite-hosted system. *Geochim et Cosmochim Acta* 92:82–99. <https://doi.org/10.1016/j.gca.2012.06.006>.
10. Lang SQ, Früh-Green GL, Bernasconi SM, Brazelton WJ, Schrenk MO, McGonigle JM. 2018. Deeply-sourced formate fuels sulfate reducers but not methanogens at Lost City hydrothermal field. *Sci Rep* 8:755. <https://doi.org/10.1038/s41598-017-19002-5>.
11. Proskurowski G, Lilley MD, Seewald JS, Früh-Green GL, Olson EJ, Lupton JE, Sylva SP, Kelley DS. 2008. Abiogenic hydrocarbon production at Lost City hydrothermal field. *Science* 319:604–607. <https://doi.org/10.1126/science.1151194>.
12. Ternieta L, Früh-Green GL, Bernasconi SM. 2021. Distribution and sources of carbon in serpentized mantle peridotites at the Atlantis Massif (IODP Expedition 357). *JGR Solid Earth* 126 e2021JB021973. <https://doi.org/10.1029/2021JB021973>.
13. McGonigle JM, Lang SQ, Brazelton WJ. 2020. Genomic evidence for formate metabolism by *Chloroflexi* as the key to unlocking deep carbon in Lost City microbial ecosystems. *Appl Environ Microbiol* 86:e02583-19. <https://doi.org/10.1128/AEM.02583-19>.
14. Motamedi S, Orcutt BN, Früh-Green GL, Twing KL, Pendleton HL, Brazelton WJ. 2020. Microbial residents of the Atlantis Massif's shallow serpentinite subsurface. *Appl Environ Microbiol* 86:e00356-20. <https://doi.org/10.1128/AEM.00356-20>.
15. Brazelton WJ, Schrenk MO, Kelley DS, Baross JA. 2006. Methane- and sulfur-metabolizing microbial communities dominate the Lost City hydrothermal field ecosystem. *Appl Environ Microbiol* 72:6257–6270. <https://doi.org/10.1128/AEM.00574-06>.
16. Brazelton WJ, Ludwig KA, Sogin ML, Andreishcheva EN, Kelley DS, Shen C-C, Edwards RL, Baross JA. 2010. Archaea and bacteria with surprising microdiversity show shifts in dominance over 1,000-year time scales in hydrothermal chimneys. *Proc Natl Acad Sci U S A* 107:1612–1617. <https://doi.org/10.1073/pnas.0905369107>.
17. Brazelton WJ, Mehta MP, Kelley DS, Baross JA. 2011. Physiological differentiation within a single-species biofilm fueled by serpentinization. *mBio* 2:e00127-11. <https://doi.org/10.1128/mBio.00127-11>.
18. Lang SQ, Lilley MD, Baumberger T, Früh-Green GL, Walker SL, Brazelton WJ, Kelley DS, Elend M, Butterfield DA, Mau AJ. 2021. Extensive decentralized hydrogen export from the Atlantis Massif. *Geology* 49:851–856. <https://doi.org/10.1130/G48322.1>.
19. Schrenk MO, Kelley DS, Bolton SA, Baross JA. 2004. Low archaeal diversity linked to subseafloor geochemical processes at the Lost City hydrothermal field, Mid-Atlantic Ridge. *Environ Microbiol* 6:1086–1095. <https://doi.org/10.1111/j.1462-2920.2004.00650.x>.
20. Bowers RM, Kyripides NC, Stepanauskas R, Harmon-Smith M, Doud D, Reddy TBK, Schulz F, Jarett J, Rivers AR, Eloe-Fadros EA, Tringe SG, Ivanova NN, Copeland A, Clum A, Becroft ED, Malmstrom RR, Birren B, Podar M, Bork P, Weinstock GM, Garrity GM, Dodsworth JA, Yoosop S, Sutton G, Glöckner FO, Gilbert JA, Nelson WC, Hallam SJ, Jungbluth SP, Ettema TJG, Tighe S, Konstantinidis KT, Liu W-T, Baker BJ, Rattei T, Eisen JA, Hedlund B, McMahon KD, Fierer N, Knight R, Finn R, Cochrane G, Karsch-Mizrachi I, Tyson GW, Rinke C, Lapidus A, Meyer F, Yilmaz P, Parks DH, Murat Eren A, Genome Standards Consortium, et al. 2017. Minimum information about a single amplified genome (MISAG) and a metagenome-assembled genome (MIMAG) of bacteria and archaea. *Nat Biotechnol* 35:725–731. <https://doi.org/10.1038/nbt.3893>.
21. Frouin E, Bes M, Ollivier B, Quéméneur M, Postec A, Debroas D, Armougom F, Erauso G. 2018. Diversity of rare and abundant prokaryotic phylotypes in the Prony hydrothermal field and comparison with other serpentinite-hosted ecosystems. *Front Microbiol* 9:102. <https://doi.org/10.3389/fmicb.2018.00102>.
22. Lecoeuvre A, Ménez B, Cannat M, Chavagnac V, Gérard E. 2021. Microbial ecology of the newly discovered serpentinite-hosted Old City hydrothermal field (southwest Indian ridge). *ISME J* 15:818–832. <https://doi.org/10.1038/s41396-020-00816-7>.
23. Costa KC, Lie TJ, Xia Q, Leigh JA. 2013. VhuD facilitates electron flow from H₂ or formate to heterodisulfide reductase in *Methanococcus maripaludis*. *J Bacteriol* 195:5160–5165. <https://doi.org/10.1128/JB.00895-13>.
24. Thauer RK, Kaster A-K, Goenrich M, Schick M, Hiromoto T, Shima S. 2010. Hydrogenases from methanogenic archaea, nickel, a novel cofactor, and H₂ storage. *Annu Rev Biochem* 79:507–536. <https://doi.org/10.1146/annurev.biochem.030508.152103>.
25. Zhou Z, Liu Y, Pan J, Cron BR, Toner BM, Anantharaman K, Breier JA, Dick GJ, Li M. 2020. Gammaproteobacteria mediating utilization of methyl-, sulfur- and petroleum organic compounds in deep ocean hydrothermal plumes. *ISME J* 14:3136–3148. <https://doi.org/10.1038/s41396-020-00745-5>.
26. Dombrowski N, Teske AP, Baker BJ. 2018. Expansive microbial metabolic versatility and biodiversity in dynamic Guaymas Basin hydrothermal sediments. *Nat Commun* 9:4999. <https://doi.org/10.1038/s41467-018-07418-0>.
27. Brazelton WJ, Baross JA. 2010. Metagenomic comparison of two thiomicrospira lineages inhabiting contrasting deep-sea hydrothermal environments. *PLoS One* 5:e13530. <https://doi.org/10.1371/journal.pone.0013530>.
28. Brazelton WJ, Nelson B, Schrenk MO. 2012. Metagenomic evidence for H₂ oxidation and H₂ production by serpentinite-hosted subsurface microbial communities. *Front Microbiol* 2:268.
29. Scott KM, Williams J, Porter CMB, Russel S, Harmer TL, Paul JH, Antonen KM, Bridges MK, Camper GJ, Campala CK, Casella LG, Chase E, Conrad JW, Cruz MC, Dunlap DS, Duran L, Fahsbender EM, Goldsmith DB, Keeley RF, Kondoff MR, Kussy BI, Lane MK, Lawler S, Leigh BA, Lewis C, Lostal LM, Marking D, Mancera PA, McClenthan EC, McIntrye EA, Mine JA, Modi S, Moore BD, Morgan WA, Nelson KM, Nguyen KN, Ogburn N, Parrino DG, Pedapudi AD, Pelham RP, Preece AM, Rampersad EA, Richardson JC, Rodgers CM, Schaffer BL, Sheridan NE, Solone MR, Staley ZR, Tabuchi M, Waide RJ, et al. 2018. Genomes of ubiquitous marine and hypersaline *Hydrogenovibrio*, *Thiomicrosrhabdus* and *Thiomicrospira* spp. encode a diversity of mechanisms to sustain chemolithotrophy in heterogeneous environments: hydrogenovibrio, Thiomicrosrhabdus, Thiomicrospira. *Environ Microbiol* 20:2686–2708. <https://doi.org/10.1111/1462-2920.14090>.
30. Kpebe A, Benvenuti M, Guendou C, Rebai A, Fernandez V, Le Laz S, Etienne E, Guigliarelli B, García-Molina G, de Lacey AL, Baffert C, Brugna M. 2018. A new mechanistic model for an O2-protected electron-bifurcating hydrogenase, Hnd from *Desulfovibrio fructosovorans*. *Biochim Biophys Acta Bioenerg* 1859:1302–1312. <https://doi.org/10.1016/j.bbabi.2018.09.364>.
31. Maia LB, Moura JJJ, Moura I. 2015. Molybdenum and tungsten-dependent formate dehydrogenases. *J Biol Inorg Chem* 20:287–309. <https://doi.org/10.1007/s00775-014-1218-2>.
32. Brazelton WJ, Thornton CN, Hyer A, Twing KL, Longino AA, Lang SQ, Lilley MD, Früh-Green GL, Schrenk MO. 2017. Metagenomic identification of active methanogens and methanotrophs in serpentinite springs of the Voltri Massif, Italy. *PeerJ* 5:e2945. <https://doi.org/10.7717/peerj.2945>.
33. Suzuki S, Nealson KH, Ishii S. 2018. Genomic and in-situ transcriptomic characterization of the candidate phylum NPL-UPL2 from highly alkaline

- highly reducing serpentized groundwater. *Front Microbiol* 9:3141. <https://doi.org/10.3389/fmicb.2018.03141>.
34. Merino N, Kawai M, Boyd ES, Colman DR, McGlynn SE, Nealson KH, Kurokawa K, Hongoh Y. 2020. Single-cell genomics of novel actinobacteria with the Wood-Ljungdahl pathway discovered in a serpentizing system. *Front Microbiol* 11:1031. <https://doi.org/10.3389/fmicb.2020.01031>.
 35. Sorokin DY, Tourova TP, Mussmann M, Muyzer G. 2008. Dethiobacter alkaliphilus gen. nov. sp. nov., and Desulfurivibrio alkaliphilus gen. nov. sp. nov.: two novel representatives of reductive sulfur cycle from soda lakes. *Extremophiles* 12:431–439. <https://doi.org/10.1007/s00792-008-0148-8>.
 36. Kaster A-K, Goenrich M, Seedorf H, Liesegang H, Wollherr A, Gottschalk G, Thauer RK. 2011. More than 200 genes required for methane formation from H₂ and CO₂ and energy conservation are present in Methanothermobacter marburgensis and Methanothermobacter thermautotrophicus. *Archaea* 2011:e973848. <https://doi.org/10.1155/2011/973848>.
 37. Fones EM, Colman DR, Kraus EA, Stepanauskas R, Templeton AS, Spear JR, Boyd ES. 2021. Diversification of methanogens into hyperalkaline serpentizing environments through adaptations to minimize oxidant limitation. *ISME J* 15:1121–1135. <https://doi.org/10.1038/s41396-020-00838-1>.
 38. Gerasimchuk AL, Shatalov AA, Novikov AL, Butorova OP, Pimenov NV, Yu LA, Yanenko AS, Karnachuk OV. 2010. The search for sulfate-reducing bacteria in mat samples from the lost city hydrothermal field by molecular cloning. *Microbiology* 79:96–105. <https://doi.org/10.1134/S0026261710010133>.
 39. Imachi H, Sekiguchi Y, Kamagata Y, Loy A, Qiu Y-L, Hugenholtz P, Kimura N, Wagner M, Ohashi A, Harada H. 2006. Non-sulfate-reducing, syntrophic bacteria affiliated with desulfotomaculum cluster i are widely distributed in methanogenic environments. *Appl Environ Microbiol* 72: 2080–2091. <https://doi.org/10.1128/AEM.72.3.2080-2091.2006>.
 40. Aquino KA, Früh-Green GL, Rickli J, Bernasconi SM, Lang SQ, Lilley MD, Butterfield DA. 2022. Multi-stage evolution of the Lost City hydrothermal vent fluids. *Geochim et Cosmochim Acta*. <https://doi.org/10.1016/j.gca.2022.06.027>.
 41. Kelley DS, Früh-Green GL. 1999. Abiogenic methane in deep-seated mid-ocean ridge environments: insights from stable isotope analyses. *J Geophys Res* 104:10439–10460. <https://doi.org/10.1029/1999JB900058>.
 42. Wang DT, Reeves EP, McDermott JM, Seewald JS, Ono S. 2018. Clumped isotopologue constraints on the origin of methane at seafloor hot springs. *Geochim et Cosmochim Acta* 223:141–158. <https://doi.org/10.1016/j.gca.2017.11.030>.
 43. Klein F, Grozeva NG, Seewald JS. 2019. Abiotic methane synthesis and serpentization in olivine-hosted fluid inclusions. *Proc Natl Acad Sci U S A* 116:17666–17672. <https://doi.org/10.1073/pnas.1907871116>.
 44. Labidi J, Young ED, Giunta T, Kohl IE, Seewald J, Tang H, Lilley MD, Früh-Green GL. 2020. Methane thermometry in deep-sea hydrothermal systems: evidence for re-ordering of doubly-substituted isotopologues during fluid cooling. *Geochim et Cosmochim Acta* 288:248–261. <https://doi.org/10.1016/j.gca.2020.08.013>.
 45. Beulig F, Røy H, McGlynn SE, Jørgensen BB. 2019. Cryptic CH₄ cycling in the sulfate–methane transition of marine sediments apparently mediated by ANME-1 archaea. *ISME J* 13:250–262. <https://doi.org/10.1038/s41396-018-0273-z>.
 46. Chadwick GL, Skennerton CT, Lasso-Pérez R, Leu AO, Speth DR, Yu H, Morgan-Lang C, Hatzepichler R, Goudeau D, Malmstrom R, Brazelton WJ, Woyke T, Hallam SJ, Tyson GW, Wegener G, Boetius A, Orphan VJ. 2022. Comparative genomics reveals electron transfer and syntrophic mechanisms differentiating methanotrophic and methanogenic archaea. *PLoS Biol* 20:e3001508. <https://doi.org/10.1371/journal.pbio.3001508>.
 47. Vekeman B, Kerckhof F-M, Cremers G, de Vos P, Vandamme P, Boon N, Op den Camp HJM, Heylen K. 2016. New Methyloceanibacter diversity from North Sea sediments includes methanotroph containing solely the soluble methane monooxygenase. *Environ Microbiol* 18:4523–4536. <https://doi.org/10.1111/1462-2920.13485>.
 48. Suzuki S, Kuenen JG, Schipper K, van der Velde S, Ishii S, Wu A, Sorokin DY, Tenney A, Meng X, Morrill PL, Kamagata Y, Muyzer G, Nealson KH. 2014. Physiological and genomic features of highly alkaliphilic hydrogen-utilizing Betaproteobacteria from a continental serpentizing site. *Nat Commun* 5:3900. <https://doi.org/10.1038/ncomms4900>.
 49. Suzuki S, Ishii S, Hoshino T, Rietze A, Tenney A, Morrill PL, Inagaki F, Kuenen JG, Nealson KH. 2017. Unusual metabolic diversity of hyperalkaliphilic microbial communities associated with subterranean serpentizing at The Cedars. *ISME J* 11:2584–2598. <https://doi.org/10.1038/ismej.2017.111>.
 50. Kohl L, Cumming E, Cox A, Rietze A, Morrissey L, Lang SQ, Richter A, Suzuki S, Nealson KH, Morrill PL. 2016. Exploring the metabolic potential of microbial communities in ultra-basic, reducing springs at The Cedars, CA, USA: experimental evidence of microbial methanogenesis and heterotrophic acetogenesis. *J Geophys Res Biogeosci* 121:1203–1220. <https://doi.org/10.1002/2015JG003233>.
 51. Miller HM, Chaudhry N, Conrad ME, Bill M, Kopf SH, Templeton AS. 2018. Large carbon isotope variability during methanogenesis under alkaline conditions. *Geochim et Cosmochim Acta* 237:18–31. <https://doi.org/10.1016/j.gca.2018.06.007>.
 52. Kraus EA, Nothaft D, Stamps BW, Rempfert KR, Ellison ET, Matter JM, Templeton AS, Boyd ES, Spear JR. 2021. Molecular evidence for an active microbial methane cycle in subsurface serpentinite-hosted groundwaters in the Samail Ophiolite, Oman. *Appl Environ Microbiol* 87:e02068-20. <https://doi.org/10.1128/AEM.02068-20>.
 53. Nobu MK, Nakai R, Tamazawa S, Mori H, Toyoda A, Ijiri A, Suzuki S, Kurokawa K, Kamagata Y, Tamaki H. 2021. Unique metabolic strategies in Hadean analogues reveal hints for primordial physiology. <https://doi.org/10.1101/2021.04.20.440570>.
 54. Smith KS, Ferry JG. 2000. Prokaryotic carbonic anhydrases. *FEMS Microbiol Rev* 24:335–366. <https://doi.org/10.1111/j.1574-6976.2000.tb00546.x>.
 55. Amend JP, Shock EL. 1998. Energetics of amino acid synthesis in hydrothermal ecosystems. *Science* 281:1659–1662. <https://doi.org/10.1126/science.281.5383.1659>.
 56. Aubrey AD, Cleaves HJ, Bada JL. 2009. The role of submarine hydrothermal systems in the synthesis of amino acids. *Orig Life Evol Biosph* 39: 91–108. <https://doi.org/10.1007/s11084-008-9153-2>.
 57. Lang SQ, Früh-Green GL, Bernasconi SM, Butterfield DA. 2013. Sources of organic nitrogen at the serpentinite-hosted Lost City hydrothermal field. *Geobiology* 11:154–169. <https://doi.org/10.1111/gbi.12026>.
 58. Dick JM, Shock EL. 2021. The release of energy during protein synthesis at ultramafic-hosted submarine hydrothermal ecosystems. *JGR Biogeosciences* 126 e2021JG006436. <https://doi.org/10.1029/2021JG006436>.
 59. Andreesen JR. 2004. Glycine reductase mechanism. *Curr Opin Chem Biol* 8:454–461. <https://doi.org/10.1016/j.cbpa.2004.08.002>.
 60. Sánchez-Andrea I, Guedes IA, Hornung B, Boeren S, Lawson CE, Sousa DZ, Bar-Even A, Claassens NJ, Stams AJM. 2020. The reductive glycine pathway allows autotrophic growth of Desulfovibrio desulfuricans. *Nat Commun* 11:5090. <https://doi.org/10.1038/s41467-020-18906-7>.
 61. Müller V, Grüber G. 2003. ATP synthases: structure, function and evolution of unique energy converters. *Cell Mol Life Sci* 60:474–494. <https://doi.org/10.1007/s000180300040>.
 62. Mei N, Postec A, Erauso G, Joseph M, Pelletier B, Payri C, Ollivier B, Quéméneur M. 2016. Serpentinella alkaliphila gen. nov., sp. nov., a novel alkaliphilic anaerobic bacterium isolated from the serpentinite-hosted Prony hydrothermal field, New Caledonia. *Int J Syst Evol Microbiol* 66:4464–4470. <https://doi.org/10.1099/ijsem.0.001375>.
 63. Postec A, Quéméneur M, Lecoeuvre A, Chabert N, Joseph M, Erauso G. 2021. Alkaliphilus serpentinus sp. nov. and Alkaliphilus pronyensis sp. nov., two novel anaerobic alkaliphilic species isolated from the serpentinite-hosted Prony Bay Hydrothermal Field (New Caledonia). *Syst Appl Microbiol* 44:126175. <https://doi.org/10.1016/j.syapm.2020.126175>.
 64. Moore WS, Frankle JD, Benítez-Nelson CR, Früh-Green GL, Lang SQ. 2021. Activities of 223Ra and 226Ra in fluids From the Lost City hydrothermal field require short fluid residence times. *JGR Oceans* 126. <https://doi.org/10.1029/2021JC017886>.
 65. Rempfert KR, Miller HM, Bompard N, Nothaft D, Matter JM, Kelemen P, Fierer N, Templeton AS. 2017. Geological and geochemical controls on subsurface microbial life in the Samail Ophiolite, Oman. *Front Microbiol* 8:56. <https://doi.org/10.3389/fmicb.2017.00056>.
 66. Nothaft DB, Templeton AS, Boyd ES, Matter JM, Stute M, Paukert Vankeuren AN, Team TODPS. 2021. Aqueous geochemical and microbial variation across discrete depth intervals in a peridotite aquifer assessed using a packer system in the Samail Ophiolite, Oman. *JGR Biogeosciences* 126. <https://doi.org/10.1029/2021JG006319>.
 67. Sabuda MC, Brazelton WJ, Putman LI, McCollom TM, Hoehler TM, Kubo MDY, Cardace D, Schrenk MO. 2020. A dynamic microbial sulfur cycle in a serpentizing continental ophiolite. *Environ Microbiol* 22:2329–2345. <https://doi.org/10.1111/1462-2920.15006>.
 68. Woychee KM, Meyer-Dombard DR, Cardace D, Argayosa AM, Arcilla CA. 2015. Out of the dark: transitional subsurface-to-surface microbial diversity in a terrestrial serpentizing seep (Manleluag, Pangasinan, the Philippines). *Front Microbiol* 6. <https://doi.org/10.3389/fmicb.2015.00044>.
 69. Cook MC, Blank JG, Rietze A, Suzuki S, Nealson KH, Morrill PL. 2021. A geochemical comparison of three terrestrial sites of serpentization: the

- Tablelands, the Cedars, and Aqua de Ney. *JGR Biogeosciences* 126. <https://doi.org/10.1029/2021JG006316>.
70. Trutschel LR, Chadwick GL, Kruger B, Blank JG, Brazelton WJ, Dart ER, Rowe AR. 2022. Investigation of microbial metabolisms in an extremely high pH marine-like terrestrial serpentizing system: Ney Springs. *Sci Total Environ* 836:155492. <https://doi.org/10.1016/j.scitotenv.2022.155492>.
 71. Schut GJ, Boyd ES, Peters JW, Adams MW. 2013. The modular respiratory complexes involved in hydrogen and sulfur metabolism by heterotrophic hyperthermophilic archaea and their evolutionary implications. *FEMS Microbiol Rev* 37:182–203. <https://doi.org/10.1111/j.1574-6976.2012.00346.x>.
 72. Nobu MK, Narihiro T, Rinke C, Kamagata Y, Tringe SG, Woyke T, Liu W-T. 2015. Microbial dark matter ecogenomics reveals complex synergistic networks in a methanogenic bioreactor. *ISME J* 9:1710–1722. <https://doi.org/10.1038/ismej.2014.256>.
 73. Youssef NH, Farag IF, Rudy S, Mulliner A, Walker K, Caldwell F, Miller M, Hoff W, Elshahed M. 2019. The Wood-Ljungdahl pathway as a key component of metabolic versatility in candidate phylum Bipolaricaulota (Acetothermia, OP1). *Environ Microbiol Rep* 11:538–547. <https://doi.org/10.1111/1758-2229.12753>.
 74. Suzuki S, Ishii S, Wu A, Cheung A, Tenney A, Wanger G, Kuenen JG, Nealson KH. 2013. Microbial diversity in The Cedars, an ultrabasic, ultra-reducing, and low salinity serpentizing ecosystem. *Proc Natl Acad Sci U S A* 110:15336–15341. <https://doi.org/10.1073/pnas.1302426110>.
 75. Amend JP, McCollom TM, Hentscher M, Bach W. 2011. Catabolic and anabolic energy for chemolithoautotrophs in deep-sea hydrothermal systems hosted in different rock types. *Geochim et Cosmochim Acta* 75: 5736–5748. <https://doi.org/10.1016/j.gca.2011.07.041>.
 76. Jain S, Dietrich HM, Müller V, Basen M. 2020. Formate is required for growth of the thermophilic acetogenic bacterium *Thermoanaerobacter kivui* lacking hydrogen-dependent carbon dioxide reductase (HDCR). *Front Microbiol* 11:59. <https://doi.org/10.3389/fmicb.2020.00059>.
 77. Zelcbuch L, Lindner SN, Zegman Y, Vainberg Slutskin I, Antonovsky N, Gleizer S, Milo R, Bar-Even A. 2016. Pyruvate formate-lyase enables efficient growth of *Escherichia coli* on Acetate and formate. *Biochemistry* 55:2423–2426. <https://doi.org/10.1021/acs.biochem.6b00184>.
 78. Cabrol NA. 2018. The coevolution of life and environment on Mars: an ecosystem perspective on the robotic exploration of biosignatures. *Astrobiology* 18:1–27. <https://doi.org/10.1089/ast.2017.1756>.
 79. Schulte M, Blake D, Hoehler T, McCollom T. 2006. Serpentization and its implications for life on the early Earth and Mars. *Astrobiology* 6: 364–376. <https://doi.org/10.1089/ast.2006.6.364>.
 80. Waite JH, Glein CR, Perryman RS, Teolis BD, Magee BA, Miller G, Grimes J, Perry ME, Miller KE, Bouquet A, Lunine JL, Brockwell T, Bolton SJ. 2017. Cassini finds molecular hydrogen in the Enceladus plume: evidence for hydrothermal processes. *Science* 356:155–159. <https://doi.org/10.1126/science.aai8703>.
 81. Jones RM, Goordial JM, Orcutt BN. 2018. Low energy subsurface environments as extraterrestrial analogs. *Front Microbiol* 9:1605. <https://doi.org/10.3389/fmicb.2018.01605>.
 82. Michalski JR, Onstott TC, Mojzsis SJ, Mustard J, Chan QHS, Niles PB, Johnson SS. 2018. The Martian subsurface as a potential window into the origin of life. *Nature Geosci* 11:21–26. <https://doi.org/10.1038/s41561-017-0015-2>.
 83. Lang SQ, Benitez-Nelson B. 2021. Hydrothermal organic geochemistry (HOG) sampler for deployment on deep-sea submersibles. *Deep Sea Res Part I: Oceanographic Res Papers* 173:103529. <https://doi.org/10.1016/j.dsr.2021.103529>.
 84. Butterfield DA, Massoth GJ. 1994. Geochemistry of north Cleft segment vent fluids: temporal changes in chlorinity and their possible relation to recent volcanism. *J Geophys Res* 99:4951–4968. <https://doi.org/10.1029/93JB02798>.
 85. Porter KG, Feig YS. 1980. The use of DAPI for identifying and counting aquatic microflora1. *Limnol Oceanogr* 25:943–948. <https://doi.org/10.4319/lo.1980.25.5.00943>.
 86. Kozich JJ, Westcott SL, Baxter NT, Highlander SK, Schloss PD. 2013. Development of a dual-index sequencing strategy and curation pipeline for analyzing amplicon sequence data on the MiSeq Illumina sequencing platform. *Appl Environ Microbiol* 79:5112–5120. <https://doi.org/10.1128/AEM.01043-13>.
 87. Callahan BJ, McMurdie PJ, Rosen MJ, Han AW, Johnson AJA, Holmes SP. 2016. DADA2: high-resolution sample inference from Illumina amplicon data. *Nat Methods* 13:581–583. <https://doi.org/10.1038/nmeth.3869>.
 88. Martin M. 2011. Cutadapt removes adapter sequences from high-throughput sequencing reads. *EMBnet j* 17:10–12. <https://doi.org/10.14806/ej.17.1.200>.
 89. Davis NM, Proctor DM, Holmes SP, Relman DA, Callahan BJ. 2018. Simple statistical identification and removal of contaminant sequences in marker-gene and metagenomics data. *Microbiome* 6:226. <https://doi.org/10.1186/s40168-018-0605-2>.
 90. Quast C, Pruesse E, Yilmaz P, Gerken J, Schweer T, Yarza P, Peplies J, Glöckner FO. 2012. The SILVA ribosomal RNA gene database project: improved data processing and web-based tools. *Nucleic Acids Res* 41: D590–596. <https://doi.org/10.1093/nar/gks1219>.
 91. Yilmaz P, Parfrey LW, Yarza P, Gerken J, Pruesse E, Quast C, Schweer T, Peplies J, Ludwig W, Glöckner FO. 2014. The SILVA and “All-species Living Tree Project (LTP)” taxonomic frameworks. *Nucleic Acids Res* 42: D643–D648. <https://doi.org/10.1093/nar/gkt1209>.
 92. McMurdie PJ, Holmes S. 2013. Phyloseq: an R package for reproducible interactive analysis and graphics of microbiome census data. *PLoS One* 8:e61217. <https://doi.org/10.1371/journal.pone.0061217>.
 93. Love MI, Huber W, Anders S. 2014. Moderated estimation of fold change and dispersion for RNA-seq data with DESeq2. *Genome Biol* 15:550. <https://doi.org/10.1186/s13059-014-0550-8>.
 94. Thornton CN, Tanner WD, VanDerslice JA, Brazelton WJ. 2020. Localized effect of treated wastewater effluent on the resistome of an urban watershed. *GigaScience* 9. <https://doi.org/10.1093/gigascience/giaa125>.
 95. Bushnell B, Rood J, Singer E. 2017. BBMerge – accurate paired shotgun read merging via overlap. *PLoS One* 12:e0185056–15. <https://doi.org/10.1371/journal.pone.0185056>.
 96. Kopylova E, Noé L, Touzet H. 2012. SortMeRNA: fast and accurate filtering of ribosomal RNAs in metatranscriptomic data. *Bioinformatics* 28: 3211–3217. <https://doi.org/10.1093/bioinformatics/bts611>.
 97. Menzel P, Ng KL, Krogh A. 2016. Fast and sensitive taxonomic classification for metagenomics with Kaiju. *Nat Commun* 7:11257. <https://doi.org/10.1038/ncomms11257>.
 98. Li D, Luo R, Liu CM, Leung CM, Ting HF, Sadakane K, Yamashita H, Lam TW. 2016. MEGAHIT v1.0: a fast and scalable metagenome assembler driven by advanced methodologies and community practices. *Methods* 102:3–11. <https://doi.org/10.1016/j.jymeth.2016.02.020>.
 99. Hyatt D, Chen G-L, LoCascio PF, Land ML, Larimer FW, Hauser LJ. 2010. Prodigal: prokaryotic gene recognition and translation initiation site identification. *BMC Bioinformatics* 11:119. <https://doi.org/10.1186/1471-2105-11-119>.
 100. Buchfink B, Reuter K, Drost HG. 2021. Sensitive protein alignments at tree-of-life scale using DIAMOND. *Nat Methods* 18:366–368. <https://doi.org/10.1038/s41592-021-01101-x>.
 101. Nurk S, Meleshko D, Korobeynikov A, Pevzner PA. 2017. metaSPAdes: a new versatile metagenomic assembler. *Genome Res* 27:824–834. <https://doi.org/10.1101/gr.213959.116>.
 102. Arkin AP, Cottingham RW, Henry CS, Harris NL, Stevens RL, Maslov S, Dehal P, Ware D, Perez F, Canon S, Sneddon MW, Henderson ML, Riehl WJ, Murphy-Olson D, Chan SY, Kamimura RT, Kumari S, Drake MM, Brettin TS, Glass EM, Chivian D, Gunter D, Weston DJ, Allen BH, Baumohr J, Best AA, Bowen B, Brenner SE, Bun CC, Chandonia JM, Chia JM, Colasanti R, Conrad N, Davis JJ, Davison BH, DeJongh M, Devoid S, Dietrich E, Dubchak I, Edirisinghe JN, Fang G, Faria JP, Frybarger PM, Gerlach W, Gerstein M, Greiner A, Gurtowski J, Haun HL, He F, Jain R, et al. 2018. KBase: the United States Department of Energy Systems Biology Knowledgebase. *Nat Biotechnol* 36:566–569. <https://doi.org/10.1038/nbt.4163>.
 103. Graham ED, Heidelberg JF, Tully BJ. 2017. BinSanity: unsupervised clustering of environmental microbial assemblies using coverage and affinity propagation. *PeerJ* 5:e3035. <https://doi.org/10.7717/peerj.3035>.
 104. Wu Y-W, Simmons BA, Singer SW. 2016. MaxBin 2.0: an automated binning algorithm to recover genomes from multiple metagenomic datasets. *Bioinformatics* 32:605–607. <https://doi.org/10.1093/bioinformatics/btv638>.
 105. Kang DD, Li F, Kirton E, Thomas A, Egan R, An H, Wang Z. 2019. MetaBAT 2: an adaptive binning algorithm for robust and efficient genome reconstruction from metagenome assemblies. *PeerJ* 7:e7359. <https://doi.org/10.7717/peerj.7359>.
 106. Sieber CMK, Probst AJ, Sharrar A, Thomas BC, Hess M, Tringe SG, Banfield JF. 2018. Recovery of genomes from metagenomes via a dereplication, aggregation and scoring strategy. *Nat Microbiol* 3:836–843. <https://doi.org/10.1038/s41564-018-0171-1>.

107. Chaumeil P-A, Mussig AJ, Hugenholz P, Parks DH. 2019. GTDB-Tk: a toolkit to classify genomes with the Genome Taxonomy Database. *Bioinformatics* 36:1925–1927. <https://doi.org/10.1093/bioinformatics/btz848>.
108. Mirdita M, Steinegger M, Breitwieser F, Söding J, Levy Karin E. 2021. Fast and sensitive taxonomic assignment to metagenomic contigs. *Bioinformatics* 37:3029–3031. <https://doi.org/10.1093/bioinformatics/btab184>.
109. Seemann T. 2014. Prokka: rapid prokaryotic genome annotation. *Bioinformatics* 30:2068–2069. <https://doi.org/10.1093/bioinformatics/btu153>.
110. Kanehisa M, Sato Y, Morishima K. 2016. BlastKOALA and GhostKOALA: KEGG tools for functional characterization of genome and metagenome sequences. *J Mol Biol* 428:726–731. <https://doi.org/10.1016/j.jmb.2015.11.006>.
111. Jones P, Binns D, Chang H-Y, Fraser M, Li W, McAnulla C, McWilliam H, Maslen J, Mitchell A, Nuka G, Pesceat S, Quinn AF, Sangrador-Vegas A, Scheremetjew M, Yong S-Y, Lopez R, Hunter S. 2014. InterProScan 5: genome-scale protein function classification. *Bioinformatics* 30:1236–1240. <https://doi.org/10.1093/bioinformatics/btu031>.
112. Søndergaard D, Pedersen CNS, Greening C. 2016. HydDB: a web tool for hydrogenase classification and analysis. *Sci Rep* 6:34212. <https://doi.org/10.1038/srep34212>.
113. Garber AI, Nealson KH, Okamoto A, McAllister SM, Chan CS, Barco RA, Merino N. 2020. FeGenie: a comprehensive tool for the identification of iron genes and iron gene neighborhoods in genome and metagenome assemblies. *Front Microbiol* 11:37. <https://doi.org/10.3389/fmicb.2020.00037>.
114. Zhang H, Yohe T, Huang L, Entwistle S, Wu P, Yang Z, Busk PK, Xu Y, Yin Y. 2018. dbCAN2: a meta server for automated carbohydrate-active enzyme annotation. *Nucleic Acids Res* 46:W95–W101. <https://doi.org/10.1093/nar/gky418>.
115. Parks DH, Imelfort M, Skennerton CT, Hugenholz P, Tyson GW. 2015. CheckM: assessing the quality of microbial genomes recovered from isolates, single cells, and metagenomes. *Genome Res* 25:1043–1055. <https://doi.org/10.1101/gr.186072.114>.
116. Eren AM, Kiefl E, Shaiber A, Veseli I, Miller SE, Schechter MS, Fink I, Pan JN, Yousef M, Fogarty EC, Trigodet F, Watson AR, Esen ÖC, Moore RM, Clayssen Q, Lee MD, Kivenson V, Graham ED, Merrill BD, Karkman A, Blankenberg D, Eppley JM, Sjödin A, Scott JJ, Vázquez-Campos X, McKay LJ, McDaniel EA, Stevens SLR, Anderson RE, Fuessel J, Fernandez-Guerra A, Maignien L, Delmont TO, Willis AD. 2021. Community-led, integrated, reproducible multi-omics with anvi'o. *Nat Microbiol* 6:3–6. <https://doi.org/10.1038/s41564-020-00834-3>.
117. Eren AM, Esen ÖC, Quince C, Vineis JH, Morrison HG, Sogin ML, Delmont TO. 2015. Anvi'o: an advanced analysis and visualization platform for 'omics data. *PeerJ* 3:e1319. <https://doi.org/10.7717/peerj.1319>.
118. Langmead B, Salzberg SL. 2012. Fast gapped-read alignment with Bowtie 2. *Nat Methods* 9:357–359. <https://doi.org/10.1038/nmeth.1923>.
119. Broad Institute. 2019. Picard Toolkit. <https://github.com/broadinstitute/picard>.
120. Quinlan AR, Hall IM. 2010. BEDTools: a flexible suite of utilities for comparing genomic features. *Bioinformatics* 26:841–842. <https://doi.org/10.1093/bioinformatics/btq033>.
121. Pruesse E, Peplies J, Glöckner FO. 2012. SINA: accurate high-throughput multiple sequence alignment of ribosomal RNA genes. *Bioinformatics* 28:1823–1829. <https://doi.org/10.1093/bioinformatics/bts252>.
122. Stamatakis A. 2014. RAxML version 8: a tool for phylogenetic analysis and post-analysis of large phylogenies. *Bioinformatics* 30:1312–1313. <https://doi.org/10.1093/bioinformatics/btu033>.
123. Madeira F, Park YM, Lee J, Buso N, Gur T, Madhusoodanan N, Basutkar P, Tivey ARN, Potter SC, Finn RD, Lopez R. 2019. The EMBL-EBI search and sequence analysis tools APIs in 2019. *Nucleic Acids Res* 47:W636–W641. <https://doi.org/10.1093/nar/gkz268>.